


AD-A272 011

FEDERAL ACQUISITION REGULATION (FAR)

		N PAGE		Form Approved OMB No. 3704-0188	
<small>Public reporting burden for this collection of information is estimated to average 1 hour per response, including the time for reviewing instructions, searching existing data sources, gathering and maintaining the data needed, and completing and reviewing the collection of information. Send comments regarding this burden estimate or any other aspect of this collection of information, including suggestions for reducing this burden, to Washington Headquarters Services, Directorate for Information Operations and Reports, 1215 Jefferson Davis Highway, Suite 1204, Arlington, VA 22202-4302, and to the Office of Management and Budget, Paperwork Reduction Project (0704-0188), Washington, DC 20503.</small>					
1. AGENCY USE ONLY (Leave blank)		2. REPORT DATE June 30, 1993		3. REPORT TYPE AND DATES COVERED Final, April 14, 1989-March 30, 1993	
4. TITLE AND SUBTITLE Low-Reynolds-Number Turbulent Boundary Layers				5. FUNDING NUMBERS 2307- DS PE61102F G-AFOSR-89-0324	
6. AUTHOR(S) Ting Wang					
7. PERFORMING ORGANIZATION NAME(S) AND ADDRESS(ES) Department of Mechanical Engineering Clemson University Clemson, SC 29634-0921				8. PERFORMING ORGANIZATION REPORT NUMBER AFOSR-TR	
9. SPONSORING/MONITORING AGENCY NAME(S) AND ADDRESS(ES) Air Force Office of Scientific Research AFOSR/NA Bolling AFB, DC 20332-6448				10. SPONSORING/MONITORING AGENCY REPORT NUMBER G-AFOSR-89-0324	
11. SUPPLEMENTARY NOTES Project Manager Major Daniel B. Fant, Air Force Office of Scientific Research					
12a. DISTRIBUTION/AVAILABILITY STATEMENT Unclassified - Unlimited This document has been approved for public release and sale; its distribution is unlimited.				12b. DISTRIBUTION CODE DTIC ELECTE NOV 03 1993 A	
13. ABSTRACT (Maximum 200 words) An experimental investigation was performed to determine the Reynolds analogy factor and turbulent Prandtl number in the transitional and low-Reynolds-number turbulent boundary layer. A miniature three-wire probe was specially designed to measure the mean velocity and temperature profiles and the Reynolds stresses and heat fluxes. Tests were conducted over a heated flat wall with zero pressure gradient and three levels of streamwise acceleration: $K = 0.07, 0.16, \text{ and } 0.25 \times 10^{-6}$. Mean temperature profiles lagged in development compared to the mean velocity profiles and the values of the Reynolds analogy factor, $2St/C_f$, in the late-transition and early-turbulent regions were lower than the values known to apply to the high-Reynolds-number turbulent flow. The profiles of Reynolds cross-stream heat flux showed negative values in the near wall region. The region of negative $\overline{v_t}$ narrowed as the flow proceeded downstream. These negative values of $\overline{v_t}$ in a flow with a negative mean temperature gradient result in negative eddy thermal diffusivity and negative Pr_t . It is speculated that the negative values might be caused by the size of the sensor and the three-dimensional behavior of transition. A conditional sampling technique was utilized to separate the flow into turbulent and non-turbulent portions. Detailed flow and thermal structures were investigated.					
14. SUBJECT TERMS Boundary Layer Transition, Heat Transfer, Accelerated Flow, Turbulent Prandtl Number, Reynolds Analogy, Favorable Pressure Gradient				15. NUMBER OF PAGES 57	
				16. PRICE CODE	
17. SECURITY CLASSIFICATION OF REPORT Unclassified	18. SECURITY CLASSIFICATION OF THIS PAGE Unclassified	19. SECURITY CLASSIFICATION OF ABSTRACT Unclassified	20. LIMITATION OF ABSTRACT UL		

FINAL TECHNICAL REPORT
SUBMITTED TO
THE AIR FORCE OFFICE OF SCIENTIFIC RESEARCH
JUNE 1993

Title: Reynolds-number Turbulent Boundary Layers

Low—

Grant No.: AFOSR-89-0324

Principal Investigator: Ting Wang, Associate Professor
Department of Mechanical Engineering
Clemson University

AFOSR Program Monitor: Major Daniel B. Fant

ABSTRACT

Boundary layer transition from laminar to turbulent flow has been recognized as an important feature in the through-flow of a gas turbine (Graham, 1979 and 1984; Mayle, 1991). Heat transfer in a turbulent boundary layer with a moderate Prandtl number is typically treated as a passive process controlled by the turbulent momentum transport. For a gas turbine blade, where as much as 50-80% of the turbulent blade surface is covered with flow undergoing laminar-turbulent transition (Turner, 1971), this relation between momentum and thermal transport has not been verified. In addition, turbine blades are exposed to diverse pressure gradients that may compound these transport differences. Recognizing and understanding the fundamental mechanisms involved in transitional convective heat transfer are keys to improving the heat transfer modeling and enhancing the accuracy of thermal load predictions on gas turbine blades.

A two-dimensional heated boundary layer undergoing natural laminar-turbulent transition was investigated to isolate the effects of streamwise acceleration and to provide insight into the fundamental mechanisms of momentum and thermal transport phenomena. Tests were conducted over a heated flat wall with zero pressure gradient and

93-26595
53905

93 11 2 6 6

three levels of streamwise acceleration: $K = \frac{v}{\bar{U}_x^2} \frac{d\bar{U}_x}{dx} = 0.07, 0.16, \text{ and } 0.25 \times 10^{-6}$.

Free-stream turbulence intensities were maintained at approximately 0.5% for the baseline case and 0.4% for the accelerating cases. A miniature three-wire probe was used to measure mean velocity and temperature profiles, Reynolds stresses and heat fluxes, and Pr_t . Transition onset and end were inferred from Stanton numbers and skin friction coefficients. Conditional sampling was implemented to separate the data into turbulent and non-turbulent portions and produce intermittency distribution.

Mild acceleration delays transition onset and increases transition length in terms of distance, x , and Reynolds number based on x . Transition onset and length are relatively insensitive to acceleration in terms of momentum thickness Reynolds number. This is supported by boundary layer thickness and integral parameters which indicate that a favorable pressure gradient suppresses boundary layer growth and development in the transition region. Heat transfer rates and temperature profiles in the late-transition and early-turbulent regions lag the development of wall shear stress and velocity profiles. This lag increases as K increases indicating a slower evolution of heat transport compared to momentum transport. This results in different distributions of eddy viscosity and eddy thermal diffusivity within this region. The values of the Reynolds analogy factor, $2St/C_f$, in the late-transition and early-turbulent regions were lower than the value known to apply to the high-Reynolds-number turbulent flow.

The streamwise gradients of Reynolds normal stress, $\frac{\partial \overline{u^2}}{\partial x}$, and Reynolds heat flux, $\frac{\partial \overline{ut}}{\partial x}$, are shown to be of significant magnitude in the transition region and should not be ignored in transitional flow models. The evolution of Reynolds shear stress in transitional flow indicates that turbulent shear is generated within the boundary layer ($Y^+ = 70 \sim 100$) and imposes on the wall shear. Conditional sampling reveals that structures within the turbulent and non-turbulent portions are not simple extensions of an

Dist	Exp Dist
A-1	

equilibrium turbulent boundary layer and a laminar boundary layer, respectively. This implies that experimentally measured data should be used as a base for the turbulent and non-turbulent portions for modeling of transitional flow using intermittency function.

Nine different criterion functions for use in the heated transitional boundary layer were investigated. Inherent differences are shown to exist between the turbulence recognition capabilities of each criterion function. A criterion function based on the Reynolds shear stress, $\left(\frac{\partial uv}{\partial \tau}\right)^2$, for turbulent/non-turbulent discrimination in a heated transitional boundary layer is considered superior to a single velocity or temperature scheme.

EXECUTIVE SUMMARY

Statement of Work

The flow and thermal structures of a two-dimensional heated boundary layer undergoing natural transition from laminar to turbulent flow were investigated in detail. The primary objective of this investigation was to isolate the effects of streamwise acceleration on this process and provide insight into the fundamental mechanisms of the momentum and thermal transport phenomena using a conditional sampling technique. A specially designed miniature three-wire probe was used to measure the Reynolds stresses and heat fluxes within the transitional boundary layer. The primary conclusions from each part of the investigation is summarized below.

Experimental Facility and Equipment

Wind Tunnel

The test facility employed in this research program was previously designed and qualified by Kuan (1987). The facility was specifically designed for studies in two-dimensional boundary layer flows. A schematic of the test facility is shown in Figure 1. An open-circuit, blowing type wind tunnel is used. Air is drawn through a filter box by a

large fan and forced through an expansion duct, two grids, a honeycomb structure, a heat exchanger, a screen pack, through a contraction nozzle, and finally into the test section.

In order to provide the two dimensional flow required in this investigation, the test section was designed with a large aspect ratio of 6. The test section was a 2.4 m long by 0.91 m high by 0.15 m wide rectangular section consisting of a heated test wall, an outer observation wall, a top wall cover, and a bottom wall table. The heated test wall is discussed below.

Heated Test Wall

The 2.4 m x 0.91 m test wall was heated to approximately 25°C above the free-stream air temperature using a uniform heat flux between 250-300 W/m². A composite construction was utilized to ensure flexibility of the test wall for future streamwise curvature studies (Figure 2). The back surface of the back wall was covered with 25.4 cm of R30 Fiberglas insulation to minimize backplane conduction losses. A 4.68 mm Lexan (polycarbonate plastic) plate was used as the primary support for the test wall (back wall). Attached to the front surface of the Lexan support was a 1.5 mm thick heating pad. The heating pad consisted of a heater foil sandwiched between glass cloth and silicon rubber sheets. The heating foil was approximately 3.8 mm wide with a spacing of 1 mm between each foil pass. The foil allowed uniform joule heating over the entire pad when current from a DC power source was applied. A 1.56 mm thick aluminum sheet was bonded to the front surface of the heater pad to ensure uniformity of the heat flux. 3M-413 into the tape to allow installation of one hundred eighty-five 3-mil E-type thermocouples. The grooves were filled with a high temperature RTV to protect the thermocouples from bending stresses expected in future curvature studies. A 1.56 mm sheet of Lexan was placed on the front surface of the 3M double sided tape to provide a smooth test surface on which the air flows and measurements were taken.

The thermocouples were strategically placed along the test surface to ensure that the evolution of the transitional flow process could be obtained. Seventy-four of the

thermocouples were located along the streamwise centerline of the wall with the remaining thermocouples in cross-span locations (Figure 3). The spacing of the centerline thermocouples was 2.54 cm for the first sixty followed by 5.08 cm for the remaining centerline thermocouples. The cross-span thermocouples were uniformly distributed across the span at seven locations 25.4 cm apart. The distance between the cross-span thermocouples was 5.08 cm with fourteen thermocouples per span with the exception of the second span. For the second span, where transition was expected to begin on a flat plate, twenty-eight thermocouples were used with a spacing of 2.54 cm.

Geometry of Test Section

For the baseline case, with no acceleration, a zero pressure gradient was needed along the entire test section. To account for the growth of the boundary layer on both the inner test wall and the outer observation wall, the displacement between the two walls was increased in the streamwise direction. The width between the two walls increased approximately linearly from 15.24 cm at the inlet of the test section to 17.78 cm at the exit of the test section. By individually adjusting the support ribs, the pressure distribution inside the test section was maintained within 1 percent.

Three different favorable pressure gradients were utilized in this investigation. A constant pressure gradient parameter, K , was maintained during each case. A constant K can be directly related to the geometry of the test section. By linearly decreasing the wall separation between the inlet and exit, a relatively constant K value could be obtained. For each accelerating case, the inlet separation distance was maintained at 15.24 cm and the separation distance decreased linearly to the exit plane. An exit separation distance of 14.6 cm was used for the lowest accelerating case of $K = 0.07 \times 10^{-6}$ while an exit separation distance of 8.9 cm was used for the highest accelerating case of $K = 0.25 \times 10^{-6}$.

Three-Wire Probe

To measure the Reynolds heat fluxes in the transitional boundary layer, a miniature three-wire probe was specially designed. This three-wire probe can measure all the boundary layer data consisting of mean and fluctuating streamwise and cross-stream velocity components, mean and fluctuating temperature, and Reynolds stresses and heat fluxes. In order to make approximate point measurements and measurements close to the wall, the measuring volume of the probe was kept to a minimum. Wollaston type platinum coated tungsten wires with copper plated ends were utilized for the velocity sensors (X array). The diameter of the velocity wires were set at $2.5\text{-}\mu\text{m}$, the minimum diameter for commercially available Wollaston type tungsten coated platinum wire. An L/d ratio for the velocity wires was chosen as 200 to maintain good frequency response and to minimize support prong interference. This L/d ratio resulted in an active sensor length of 0.5 mm of the total wire length of 1 mm. A platinum temperature wire of diameter $1.25\text{-}\mu\text{m}$ was chosen as a trade-off between wire frequency response and wire durability. A smaller diameter wire has a higher frequency response but is also more fragile. The temperature wire had a length of 0.35 mm corresponding to the projected sensor length of the X array, resulting in an L/d ratio of 280.

The sensor orientation and spacing involved a trade-off between prong and sensor interference effects and spatial resolution. Blair and Bennet (1984), using similar sensor dimensions, found a wire spacing of 0.35 mm minimized cross-talk error and signal attenuation. Following their recommendations, a wire spacing of 0.35 mm was chosen. The X wires were placed orthogonal to each other while the temperature wire was made parallel to the X wire plane and normal to the mean flow direction. This orientation for the temperature wire was chosen to eliminate any streamwise temperature gradients. Also, since the temperature wire was operated in a constant current mode, this orientation simplified the data reduction equations and resulted in a lower uncertainty.

To avoid the difficulty in bending three pairs of prongs while maintaining the proper sensor arrangement as with a typical boundary layer probe. The probe support was bent instead at an angle of 10° from the probe axis. This angle was chosen to ensure that both of the X wires touched the wall simultaneously. A schematic of the probe and sensor arrangement is shown in Figure 4. A complete description of the probe design and qualification can be found in Shome (1991).

Summary of Results

Summary of the Baseline Case

The transition onset for the baseline case occurred at $Re_x = 5.5 \times 10^5$ ($Re_\theta = 492$) which is earlier than the transition onset for a FSTI value of 0.5% predicted from empirical correlations. Apparently, factors other than FSTI influence transition onset. Onset of transition was taken as the point when skin friction (and/or Stanton number) deviates from the corresponding laminar correlation (Figure 5). Measurements of the Reynolds normal stress indicated that the flow in the transition region is much less isotropic than the flow in a fully turbulent boundary layer. The Reynolds shear stress was shown to be generated within the boundary layer ($Y^+ = 70 \sim 100$) and impose on the wall shear by influencing the mean velocity profile near the wall (Figure 6). Mean temperature profiles lagged in development compared to the mean velocity profiles and the values of the Reynolds analogy factor, $2St/C_f$, in the late-transition and early-turbulent regions were lower than the 1.2 value known to apply to the high-Reynolds-number turbulent flow (Figure 7). These results indicate a slower response of heat transport in this region compared to that of momentum transport.

The streamwise gradients of the streamwise Reynolds normal stress, $\frac{\partial u^2}{\partial x}$, and the streamwise Reynolds heat flux, $\frac{\partial \overline{ut}}{\partial x}$, were shown to be of significant magnitude in the transition region and should not be ignored in transitional flow models when computational methods are used. The profiles of Reynolds cross-stream heat flux showed

negative values in the near wall region (Figure 8). The region of negative $\overline{\nu_t}$ narrowed as the flow proceeded downstream. These negative values of $\overline{\nu_t}$ in a flow with a negative mean temperature gradient result in negative eddy thermal diffusivity and negative Pr_t , which are not physically appropriate. It is speculated that the negative values might be caused by the size of the sensor and the three-dimensional behavior of transition. Different distributions of eddy viscosity and eddy thermal diffusivity were observed and reflect the apparent disparity between turbulent momentum and thermal transport mechanisms in the transitional boundary layer (Figures 9 and 10).

Summary of the Streamwise Accelerating Cases

Streamwise acceleration was shown to delay the point of transition onset both in terms of physical distance, x , and Reynolds number based on x (Figures 11 and 12). The transition onset momentum Reynolds number, $Re_{\theta S}$, was relatively insensitive to acceleration. In general, the physical length of transition increased with increasing K . However, the transition length in terms of Re_{θ} was relatively constant with increasing K (Table 1). This was supported by the boundary layer thickness and integral parameters which indicated that an increasing pressure gradient suppresses boundary layer growth and development through the transition region (Figure 13). The Reynolds normal stresses were suppressed in the near-wall region ($Y^+ < 50$) relative to the baseline case as K increased (Figures 14, 15 and 16). This was believed to be caused by a thickening of the viscous sublayer relative to the boundary layer thickness. The lag that was observed between the mean temperature profiles and the mean velocity profiles for the baseline case became more pronounced with increasing K (Figures 17 and 18). Comparison of the evolution of RMS temperature fluctuations to the evolution of Reynolds normal stresses indicated a lag in the RMS temperature fluctuations. This supported the observation from the mean temperature and velocity profiles that the thermal transport lags behind the

momentum transport in the transition region and that the effect is more pronounced as K increases.

Summary of the Conditional Sampling Technique

Nine different criterion functions for use in the heated transitional boundary layer were investigated (Figure 19). A criterion function based on Reynolds stress, $\left(\frac{\partial uv}{\partial \tau}\right)^2$, resulted in the sharpest demarcation between turbulent and non-turbulent portions of the flow (Figure 20). This criterion function also had a negligible variation of threshold value throughout the transition region with the lowest sensitivity of the resultant intermittency to the variation of the threshold (Figure 21). These results indicate that using the Reynolds shear stress for turbulent/non-turbulent discrimination in a heated transitional boundary layer is superior to a single velocity or temperature scheme. Criterion functions based on correlations schemes consistently resulted in intermittency values 0.14 to 0.38 lower in the outer boundary layer region ($y/\delta^* > 4.0$) than the values found from single signal schemes (Figure 22). No differences were found using the temperature based criterion function to support the use of a separate thermal intermittency factor in accelerating flows. Inherent differences were shown to exist between each criterion function's turbulence recognition capabilities. Each criterion function weights different areas within a turbulent burst differently. As a result, different criterion functions may result in the same overall intermittency factor but analysis of the turbulent and non-turbulent portions would not always yield the same result (Figures 23 and 24).

Peak values in intermittency for the early to mid-transitional regions were found to occur away from the wall at approximately $y/\delta = 0.3$ for the baseline case and three accelerating cases (Figure 25). To match the universal intermittency distribution of Dhawan and Narasimha (1958), the values of intermittency at the near-wall minimum $y/\delta = 0.1$ should be used as the representative "near-wall" values. For the accelerating cases, two linear regions of different slopes were observed when intermittency was presented in

$R(\Gamma)$ versus x coordinates (Figure 26). Narasimha (1985) termed this sudden change in flow behavior "subtransition" indicating the flow changes from a subcritical to a supercritical state.

Summary of the Conditional Sampling Results

The conditionally sampled distribution of the skin friction coefficients revealed values for C_f in the non-turbulent and turbulent portions significantly deviated from the respective laminar and turbulent correlations. Reconstructing the local overall C_f value using the laminar and turbulent correlations consistently overestimates the experimentally determined unconditioned C_f values (Figure 27). The results indicate that a single representative near-wall intermittency value may not be the characteristic property for the transition region and that the $\Gamma(y)$ variation may play a more important role than previously thought. Evaluation of the conditionally sampled momentum thickness confirmed that the higher loss of momentum in the transition region is a direct result of the turbulent portion of the boundary layer. The mean velocity profiles from the turbulent portions had the appearance of a low-Reynolds-number turbulent boundary layer with a large wake region (Figure 28). In the late transition region, as K increased, the wake region in the turbulent portion was suppressed relative to the unconditioned result (Figure 29).

The increased magnitude of the streamwise Reynolds normal stress was discovered to be a direct result of the fluctuations in the turbulent portions and not a result of the "mean-step" contribution (Figure 30). The peak intensity of the streamwise Reynolds normal stress in the non-turbulent portion was suppressed at an earlier stage as K increased (Figure 31). The Reynolds shear stress was normalized by the individual C_f values obtained for each portion (Figures 32 and 33). The peak magnitudes of Reynolds shear still exceeded the wall shear but not by the magnitudes seen in the baseline case. The results indicated that the turbulent shear was generated in the boundary layer at $Y^+ \approx 100$ and imposes on the wall shear and that the "mean-step" contribution was

negligible. As K increased, \overline{uv} in the turbulent portion was more uniformly distributed through the inner boundary layer than the unconditioned results (Figure 34). The peak intensity in the RMS temperature fluctuations in the non-turbulent portions increased in magnitude and eventually became greater than the turbulent and unconditioned values in the late transition region. The streamwise Reynolds heat flux in the turbulent portion increased in magnitude as K increased (Figures 35, 36, and 37).

Overall Conclusions

The development of the mean temperature profiles were shown to lag behind the development of the mean velocity profiles indicating differences in the mechanisms of thermal transport and momentum transport. This lag increased as K increased. In performing numerical analysis of transitional boundary layers, the thermal transport cannot be directly inferred from the momentum transport by a simple extension of Reynolds analogy.

The common practice of using intermittency in calculating transitional boundary layer flows requires modification. Conditional sampling of the Reynolds stresses and heat fluxes reveal that structures within the turbulent and non-turbulent portions are not simple extensions of an equilibrium turbulent boundary layer and a laminar boundary layer, respectively. Experimentally measured data should be used as a base for the turbulent and non-turbulent portions, not laminar and fully turbulent flow. The streamwise gradient terms, such as $\frac{\partial u^2}{\partial x}$ and $\frac{\partial \overline{ut}}{\partial x}$ should be retained in the boundary layer equations for numerical calculation. Also, the $\Gamma(y)$ variation may play a more important role than previously thought and using a single representative near-wall intermittency value may not be adequate.

Caution should be used when implementing a criterion function for use in a transitional boundary layer. Different criterion functions may result in the same overall

value of intermittency but the analysis of the flow and thermal structures may not have similar results.

Recommendations

The results of the present study indicate the need for further investigation of the mechanisms of transport of momentum and heat in boundary layers undergoing laminar to turbulent transition. In light of the results of the present study the following recommendations are made for future work:

1. Further investigations into the occurrence of negative cross-stream Reynolds heat flux must be performed. Two steps should be taken. First, a new design should be implemented for the three-wire probe preferably by placing the temperature sensor between the two velocity sensors in order to resolve the issue of spatial resolution. Second, the span-wise Reynolds heat flux should be measured and a local balance of the heat transport performed to more thoroughly investigate the three-dimensional transport.
2. The concept of using a single representative near-wall intermittency value requires further investigation. An experimental technique should be developed to enable simultaneous measurements within the boundary layer in a cross-stream plane. Using this technique, a single representative near-wall intermittency value could be used to separate the flow throughout the boundary layer.
3. A detailed spectral investigation for the conditionally sampled data within each portion should be performed. This would provide additional insight into the development of the cascade process within the turbulent spot during the transition process and determine the magnitude of damping of the sinusoidal oscillations in the non-turbulent portion due to streamwise acceleration.
4. The combined effects of streamwise acceleration in the presence of elevated FSTI should be performed. This will provide information into the extent of interaction between the free-stream and the accelerating boundary layer.

OTHER PERSONNEL ASSOCIATED WITH THIS PROGRAM

1. F. Jeffrey Keller, a doctoral student supported by this AFOSR grant -- He graduated with a Ph.D. in June 1993, dissertation title, "Flow and Thermal Structures in Heated Transitional Boundary Layers with and without Streamwise Acceleration".
2. Dadong Zhou, a doctoral student -- He was primarily supported by an ONR grant and had been supported by this AFOSR grant for five months. He is expected to graduate in August 1993.

3. Biswadip Shome, a masters student supported by a graduate assistantship from Clemson University -- He developed the three-wire probe to measure Reynolds stresses and heat fluxes for this program. He finished his masters program at Clemson in August 1991.

PUBLICATIONS

Refereed Journal Publications

"Effects of Different Criterion Functions on Intermittency in Heated Transitional Boundary layers with and without Streamwise Acceleration," F. J. Keller and T. Wang, accepted for publication in the ASME Journal of Turbomachinery.

"Effects of Elevated Free-Stream Turbulence on Flow and Thermal Structures in Transitional Boundary Layers," Zhou, D., and Wang, T., accepted for publication in the ASME Journal of Turbomachinery.

Refereed Conference Papers

"Effects of Different Criterion Functions on Intermittency in Heated Transitional Boundary layers with and without Streamwise Acceleration," F.J. Keller and T. Wang, ASME paper 93-GT-67, Presented at the 1993 ASME International Gas Turbine and Aeroengine Congress and Exposition, Cincinnati, Ohio.

"Effects of Elevated Free-Stream Turbulence on Flow and Thermal Structures in Transitional Boundary Layers," Zhou, D., and Wang, T., Presented at the International Gas Turbine and Aeroengine Congress and Exposition, Cincinnati, Ohio, May 24-27, 1993.

"Experimental Investigation of Reynolds Shear Stresses and Heat Fluxes in a Transitional Boundary Layer," T. Wang, F.J. Keller, and D. Zhou, ASME HTD-Vol. 226, Fundamental and Applied Heat Transfer Research for Gas Turbine Engines, pp. 61-70, 1992

"Laminar Boundary Layer Flow and Heat Transfer with Favorable Pressure Gradient at Constant K Values," Zhou, D., and Wang, T., Presented at the ASME International Gas Turbine and Aeroengine Congress and Exposition, Cologne, Germany, June 1-4, 1992, ASME paper No. 92-GT-246.

Technical Reports

"Development of Three-Wire Probe for the Measurement of Reynolds Stresses and Heat Fluxes in the Transitional Boundary Layer," T. Wang and B. Shome, August 1991.

"Flow and Thermal Structures in Heated Transitional Boundary Layers with and without Streamwise Acceleration," J. Keller and T. Wang, June 1993.

NOMENCLATURE

- C_f - skin friction coefficient, $\tau_w/(\rho \bar{U}_\infty^2/2)$
 C_p - pressure coefficient, $\frac{P_s - P_{sref}}{\frac{1}{2} \rho \bar{U}_{xref}^2}$
 d - sensor diameter
 E - voltage
 $FSTI$ - freestream turbulence intensity, $\sqrt{(u'^2 + v'^2 + w'^2)/3}/\bar{U}_x$
 H - shape factor, δ^*/θ
 K - pressure gradient parameter, $\frac{v}{\bar{U}_x^2} \frac{d\bar{U}_x}{dx}$
 L - sensor length
 M - frequency response
 n - turbulent spot production rate
 N - number of data readings
 P_s - static pressure
 Pr_t - turbulent Prandtl number, $(\overline{uv}/\partial\bar{U}/\partial y)/(\overline{vT}/\partial\bar{T}/\partial y)$
 q'' - heat flux
 Re - Reynolds number
 St - Stanton number, $q''_w/[\rho C_p \bar{U}_\infty (\bar{T}_w - \bar{T}_{ad})]$
 t - fluctuation in temperature
 T - instantaneous temperature
 \bar{T} - mean temperature
 t' - rms value of temperature fluctuations
 T^+ - $\frac{(\bar{T}_w - \bar{T}) \sqrt{\tau_w/\rho}}{q''/(\rho C_p)}$
 u, v, w - instantaneous velocity fluctuations in streamwise, cross-stream, and spanwise directions
 u', v' - rms values of velocity fluctuations

- u_τ - friction velocity, $\sqrt{\tau_w / \rho}$
 U - instantaneous velocity
 \bar{U} - mean velocity
 U^+ - \bar{U} / u_τ
 \overline{uv} - Reynolds shear stress
 \overline{ut} - Reynolds streamwise heat flux
 \overline{vt} - Reynolds cross-stream heat flux
 x - coordinate in streamwise direction
 y - coordinate normal to the surface
 Y^+ - yu_τ / ν
 Greek
 α - thermal diffusivity
 δ - boundary layer thickness at $0.995 U_e$
 δ^* - displacement thickness
 Δ_2 - enthalpy thickness
 ϵ - dissipation rate
 ϵ_H - turbulent (or eddy) thermal diffusivity
 ϵ_M - turbulent (or eddy) viscosity
 Λ - Pohlhausen pressure gradient parameter, $\frac{\theta^2}{\nu} \frac{dU_e}{dx}$
 λ - integral length scale, $\bar{U} \infty \int_0^\infty \overline{u(t)u(t+\tau)} / \overline{u^2} d\tau$
 Γ - intermittency factor
 η - dimensionless length, $\frac{Re_x - Re_{x_s}}{Re_{x_E} - Re_{x_s}}$
 ν - kinematic viscosity
 θ - momentum boundary layer thickness
 ρ - density
 τ - time

τ_w - shear stress on the wall

Subscripts

ad - adiabatic
 amb - ambient
 an - anemometer
 cl - conduction layer
 corr - corrected
 crit - critical value
 ∞ - free-stream value
 E - transition end
 nt - non-turbulent
 ref - reference location at $x = 20$ cm
 s - transition onset
 t - turbulent
 w - at the wall

REFERENCES

1. Blair, M.F., and Bennet, J.C., 1984, "Hot-Wire Measurements of Velocity and Temperature Fluctuations in a Heated Turbulent Boundary Layer," 29th ASME International Gas Turbine Conference, pp. 1-10, June 3-7, Amsterdam.
2. Dhawan, S., and Narasimha, R., 1958, "Some Properties of Boundary Layer Flow During the Transition from Laminar to Turbulent Motion," J. Fluid Mech., Vol. 3, pp. 418-436.
3. Graham, R.W., 1979, "Fundamental Mechanisms that Influence the Estimate of Heat Transfer to Gas Turbine Blades," NASA, TM-79128 or ASME Paper 79-HT-43.
4. Kuan, C.L., 1987, "An Experimental Investigation of Intermittent Behavior in the Transitional Boundary Layer," M.S. Thesis, Clemson University, Clemson, SC.
5. Mayle, R.E., 1991, "The Role of Laminar-Turbulent Transition in Gas Turbine Engines", ASME J. of Turbomachinery, Vol. 113, pp. 509.

6. Narasimha, R., 1985, "The Laminar-Turbulent Transition Zone in the Boundary Layer," *Prog. Aerospace Sci.*, 22, pp. 29-80.
7. Shome, B., 1991, "Development of a Three-Wire Probe for the Measurement of Reynolds Stresses and Heat Fluxes in Transitional Boundary Layers," M.S. Thesis, Clemson University, Clemson, SC.
8. Turner, A.B., 1971, "Local Heat Transfer Measurements on a Gas Turbine Blade," *J. of Mech. Engr. Sci.*, Vol. 13, No. 1, pp. 1-12.

Table 1 Reynolds numbers at onset and end of transition for all test cases
(Note: ****, indicates no end of transition was observed in the test facility).

		Baseline	K1=0.07x10 ⁻⁶	K2=0.16x10 ⁻⁶	K3=0.25x10 ⁻⁶
			6	6	6
FSTI at x _s		0.5	0.4	0.4	0.4
U _∞ (m/s) at Stal (x = 18 cm)		12.24	12.68	12.20	12.45
Onset of transition	x(cm)	68	107	115	122
	Re _x	5.50 x 10 ⁵	9.46 x 10 ⁵	10.3 x 10 ⁵	12.5 x 10 ⁵
	Re _{δ*}	1294	1322	1233	1233
	Re _θ	492	541	544	552
End of transition	x(cm)	137	168	213	****
	Re _x	11.2 x 10 ⁵	15.7 x 10 ⁵	21.7 x 10 ⁵	****
	Re _{δ*}	1826	1874	1880	****
	Re _θ	1302	1282	1235	****
Length of transition	x(cm)	69	61	98	****
	Re _x	5.70 x 10 ⁵	6.24 x 10 ⁵	11.4 x 10 ⁵	****
	Re _{δ*}	532	552	647	****
	Re _θ	810	741	691	****

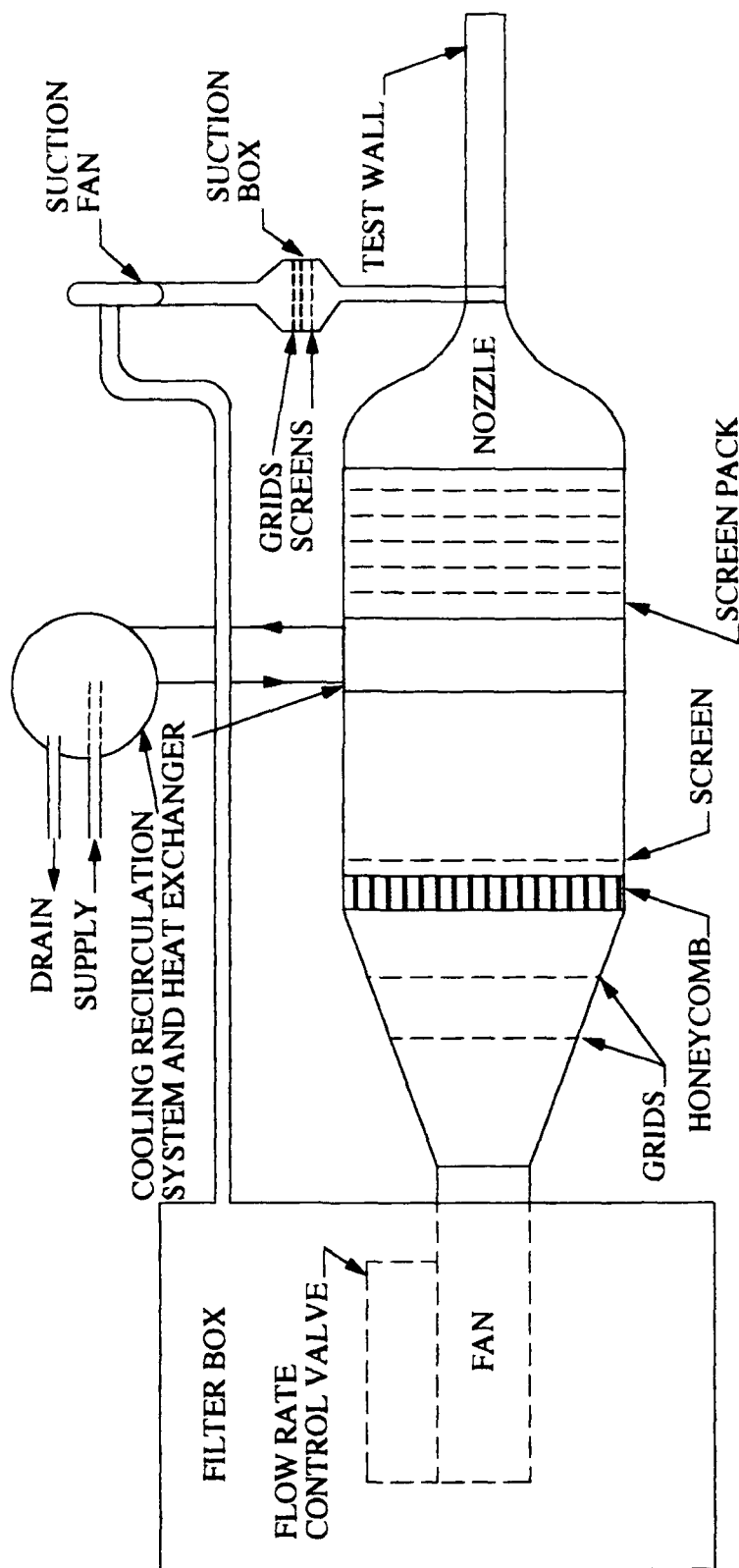


Figure 1 Schematic of wind tunnel facility.

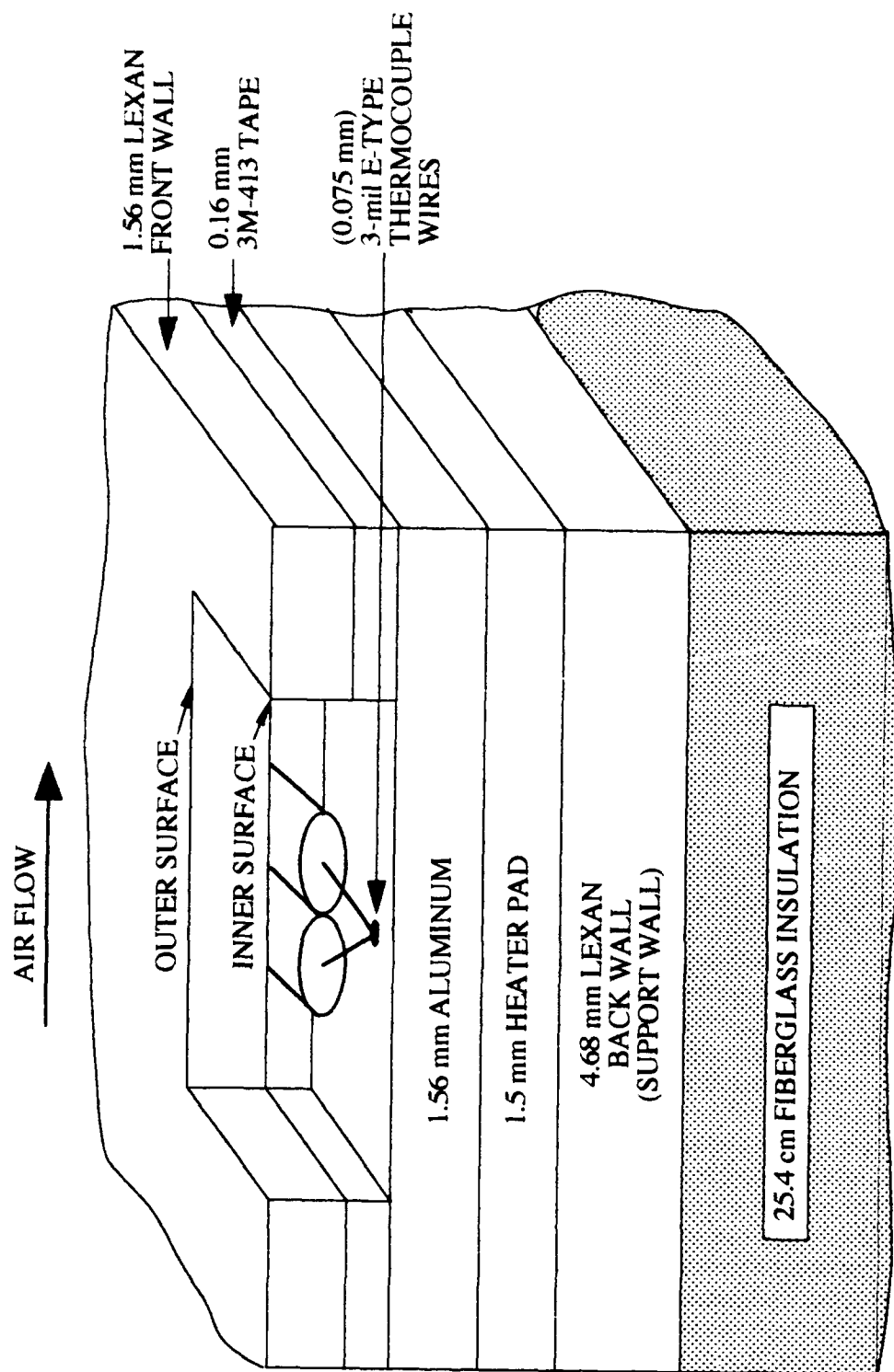


Figure 2 Schematic of composite heated test wall.

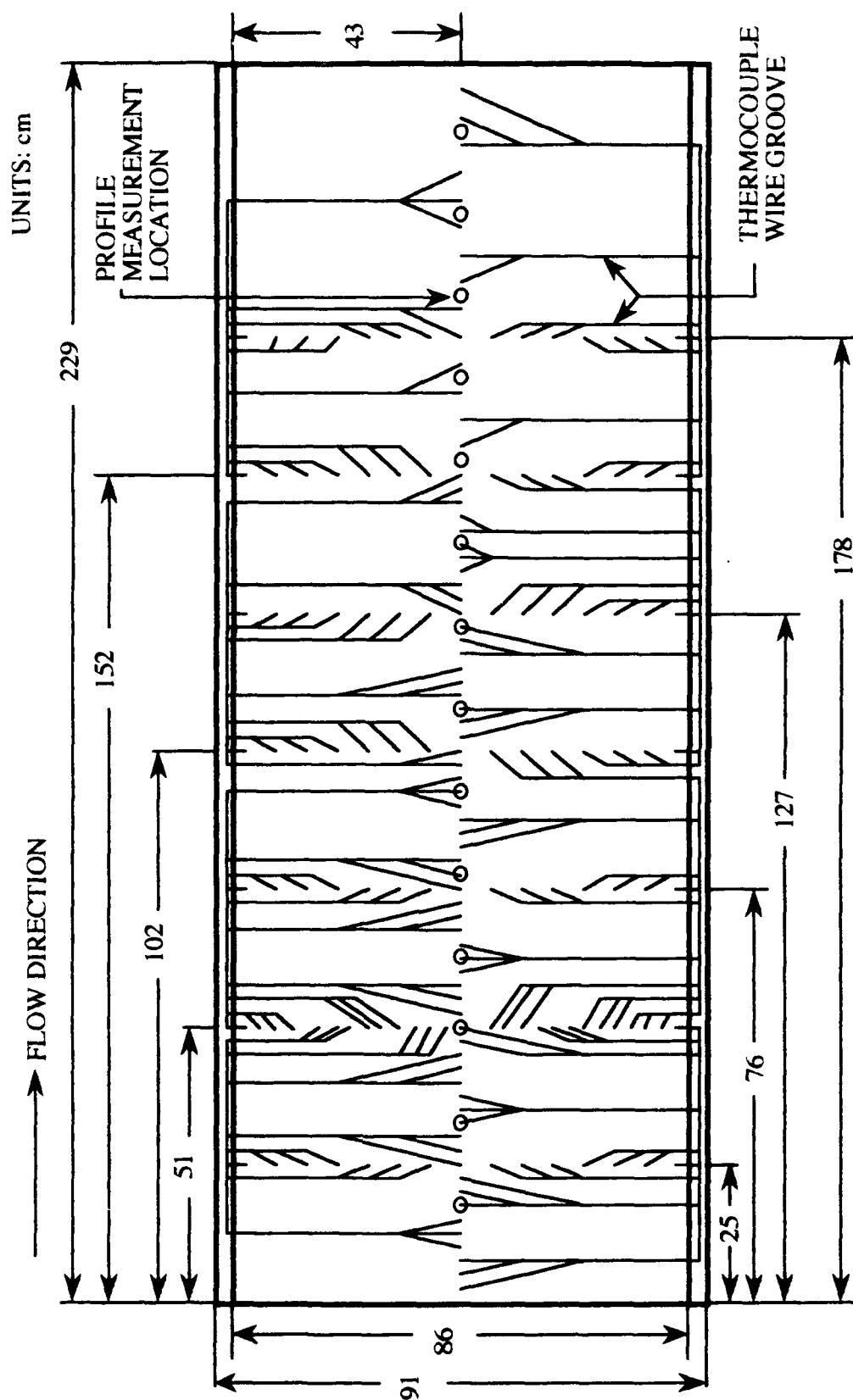
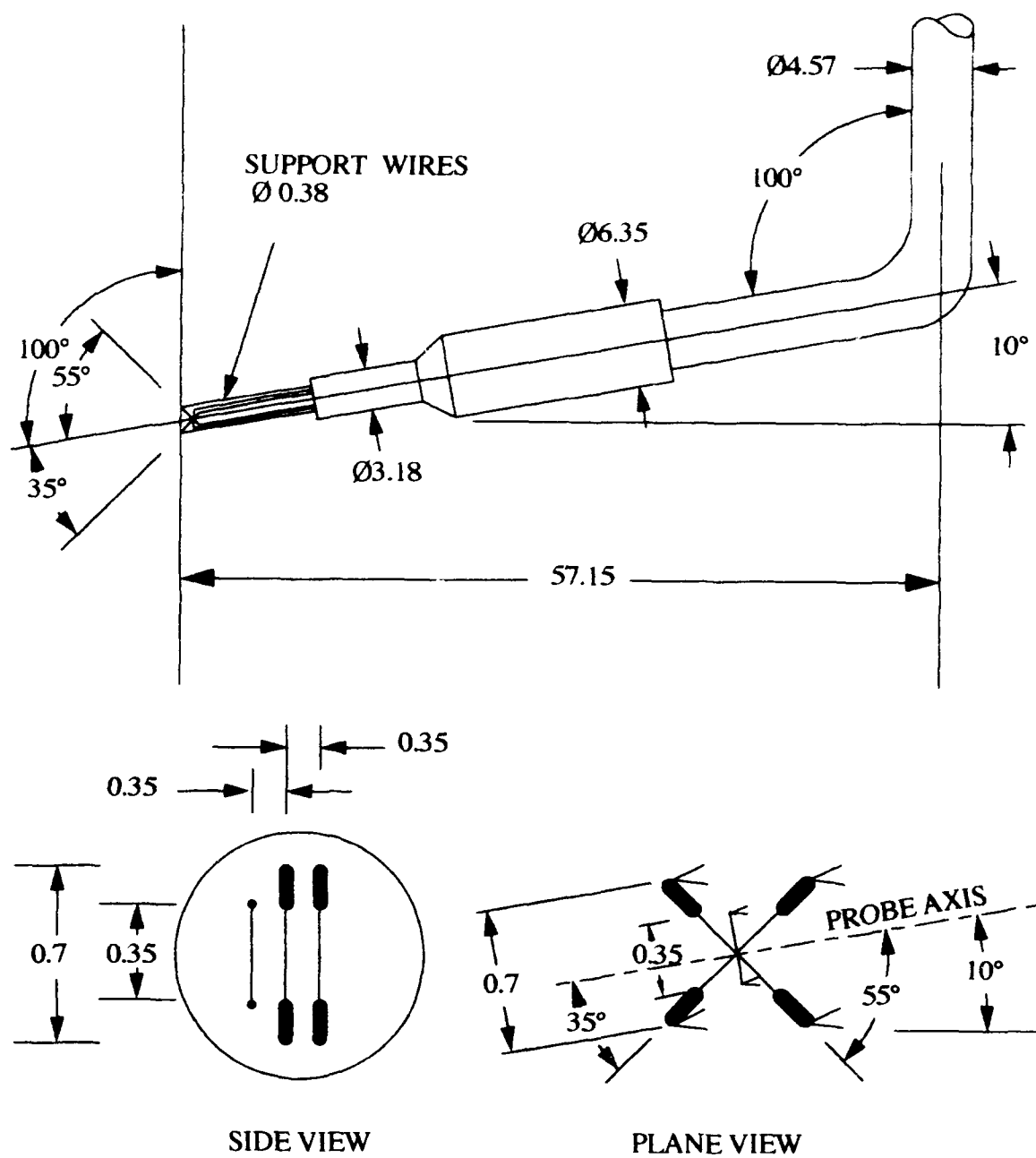


Figure 3 Schematic of thermocouple layout. o - indicates location for boundary layer measurements.



DIMENSIONS IN mm

Figure 4 3-wire boundary layer sensor for measuring Reynolds stresses and heat fluxes.

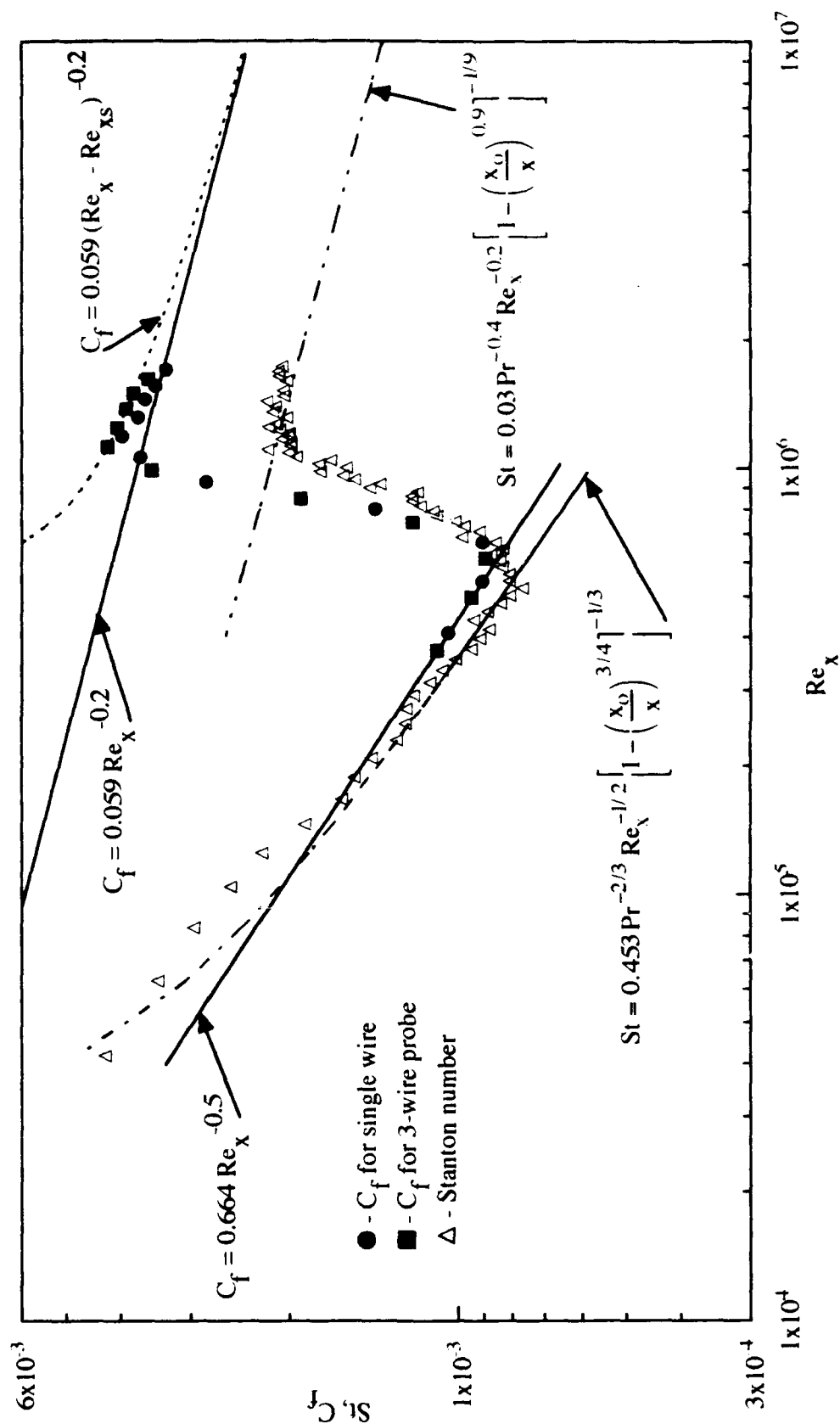


Figure 5 Centerline Stanton number and skin friction coefficient distributions for the baseline case.

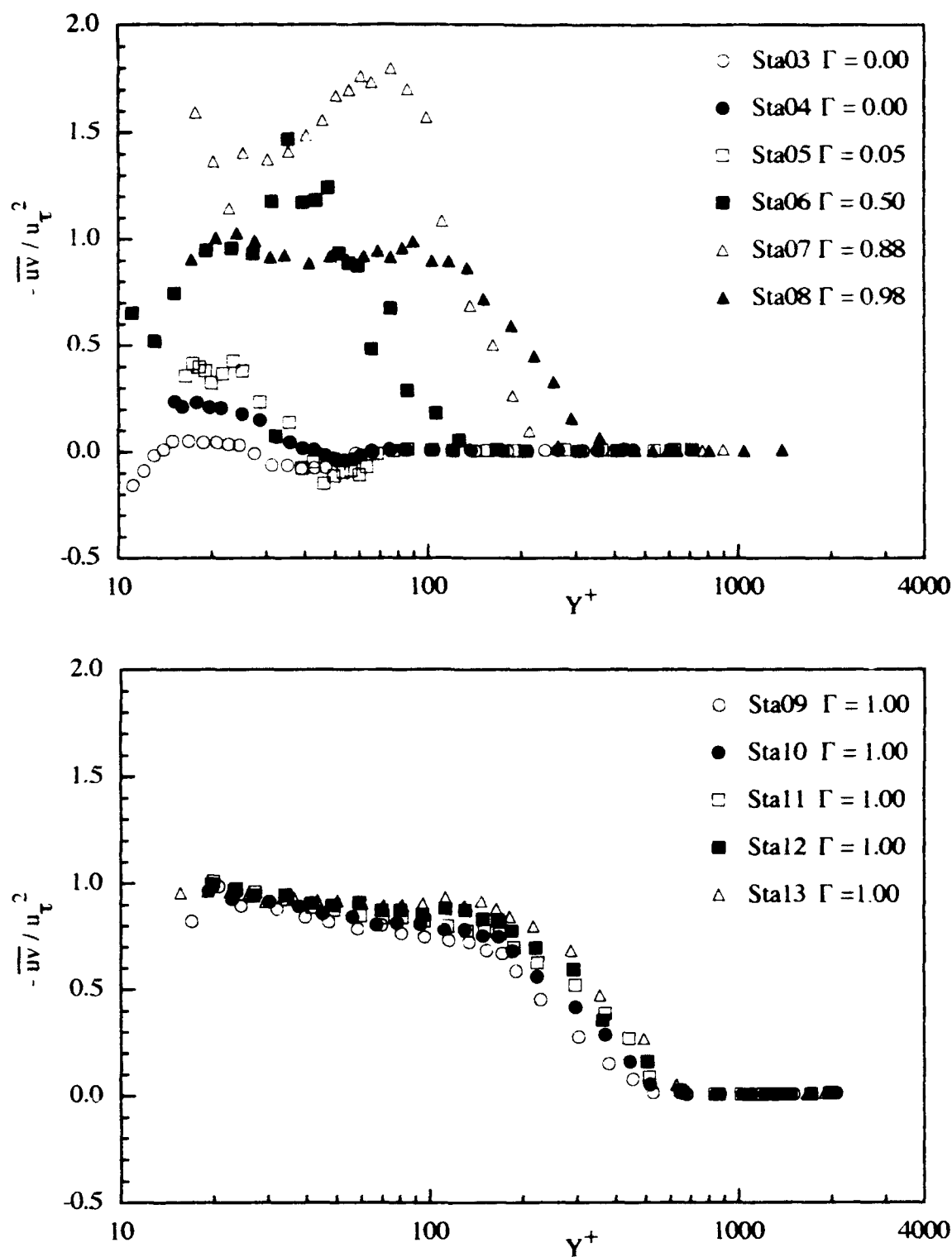


Figure 6 Reynolds shear stress distribution for the baseline case in wall units.

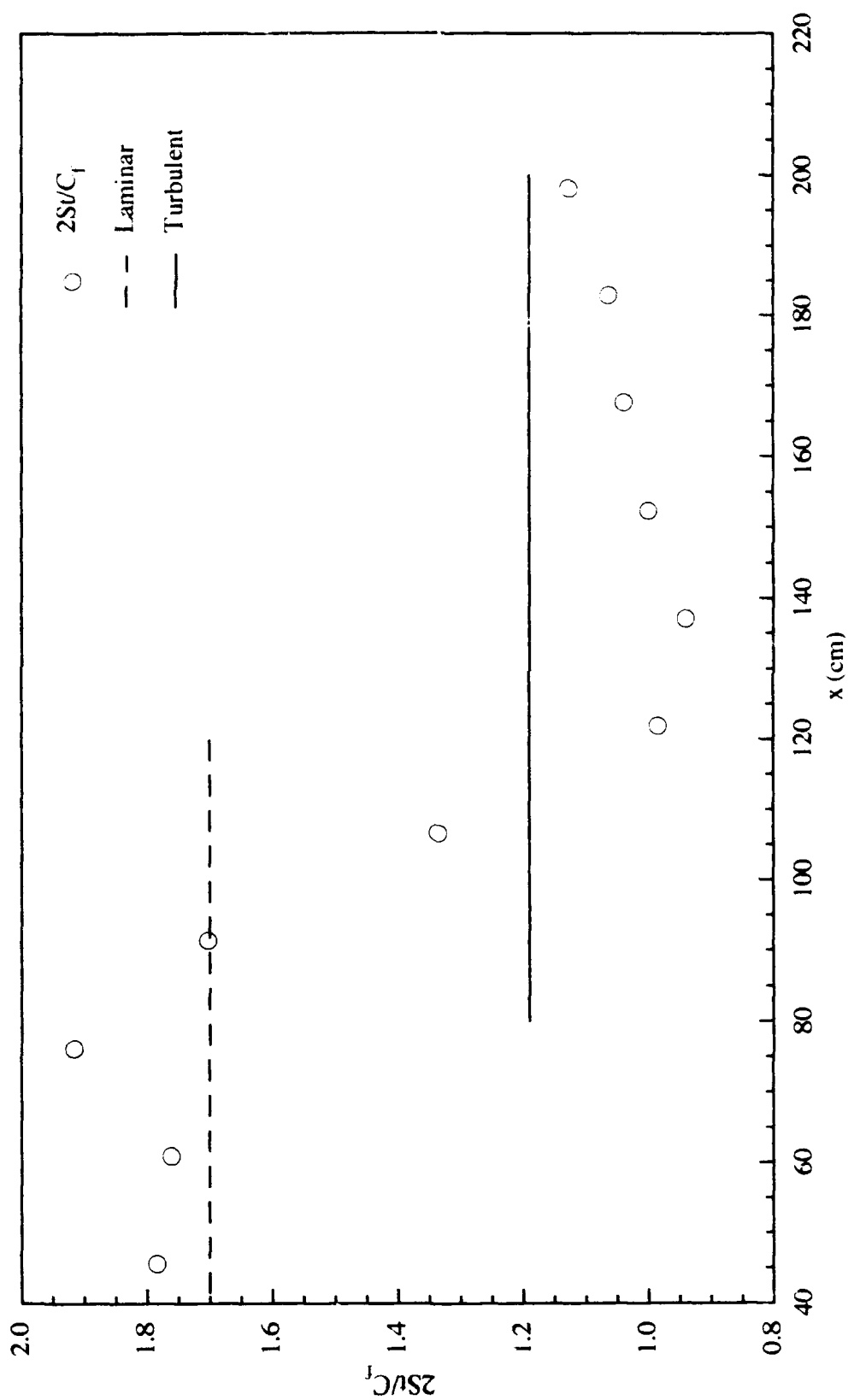


Figure 7 Reynolds analogy factor, $2St/C_f$, for the baseline case.

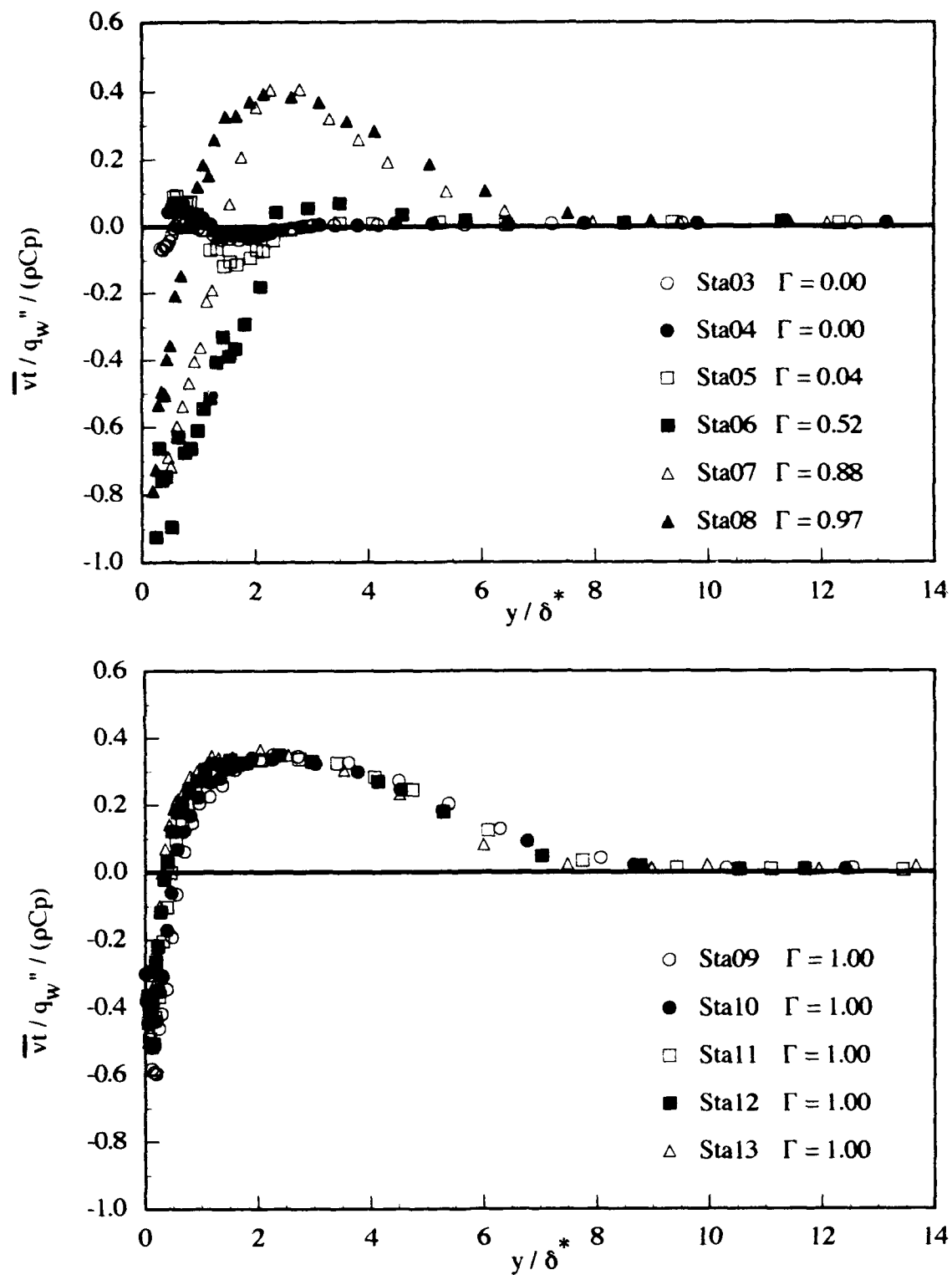


Figure 8 Cross-Stream Reynolds heat flux distribution for the baseline case.

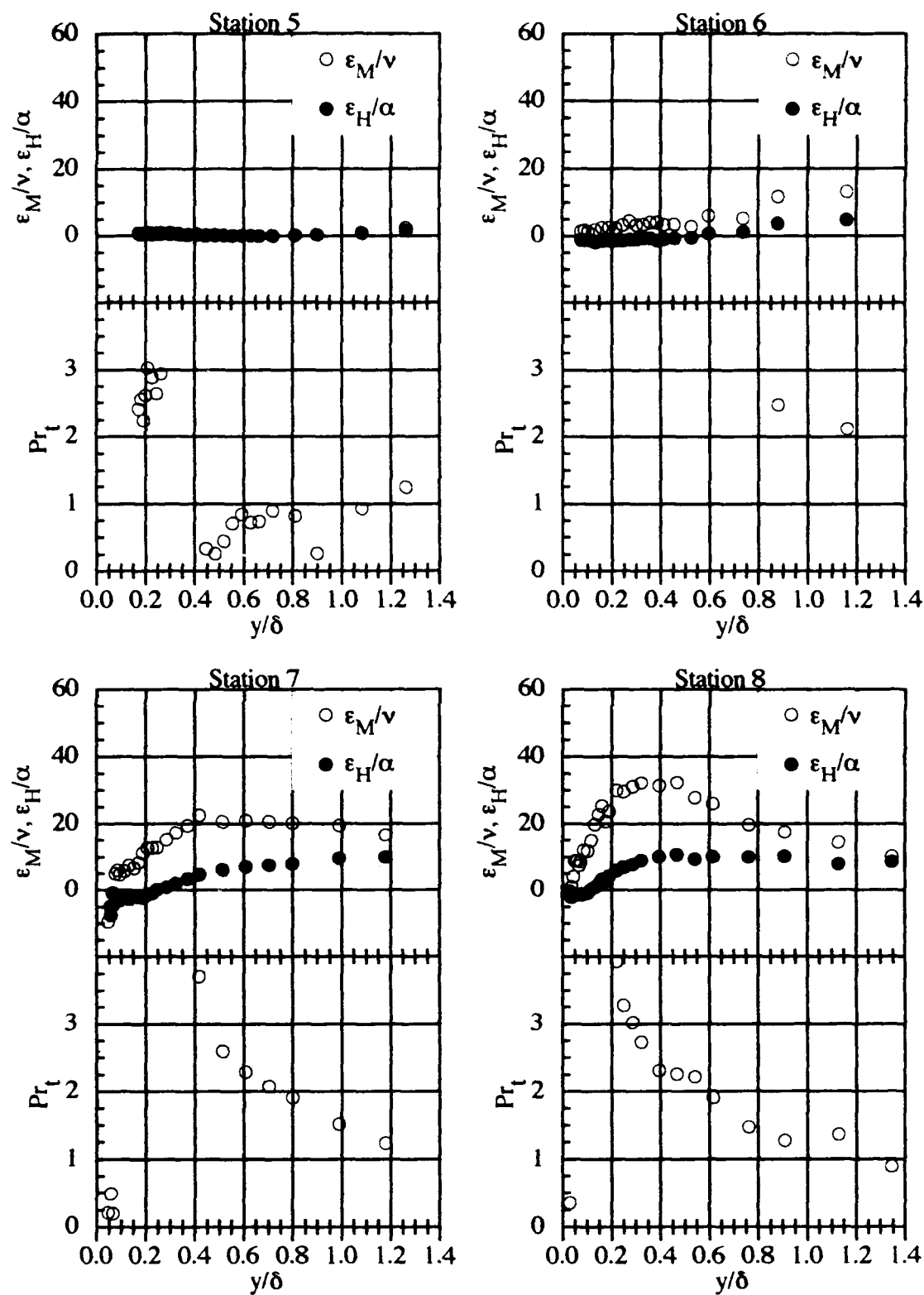


Figure 9 Distribution of eddy viscosity, turbulent thermal diffusivity and turbulent Prandtl number for baseline case (stations 5-8).

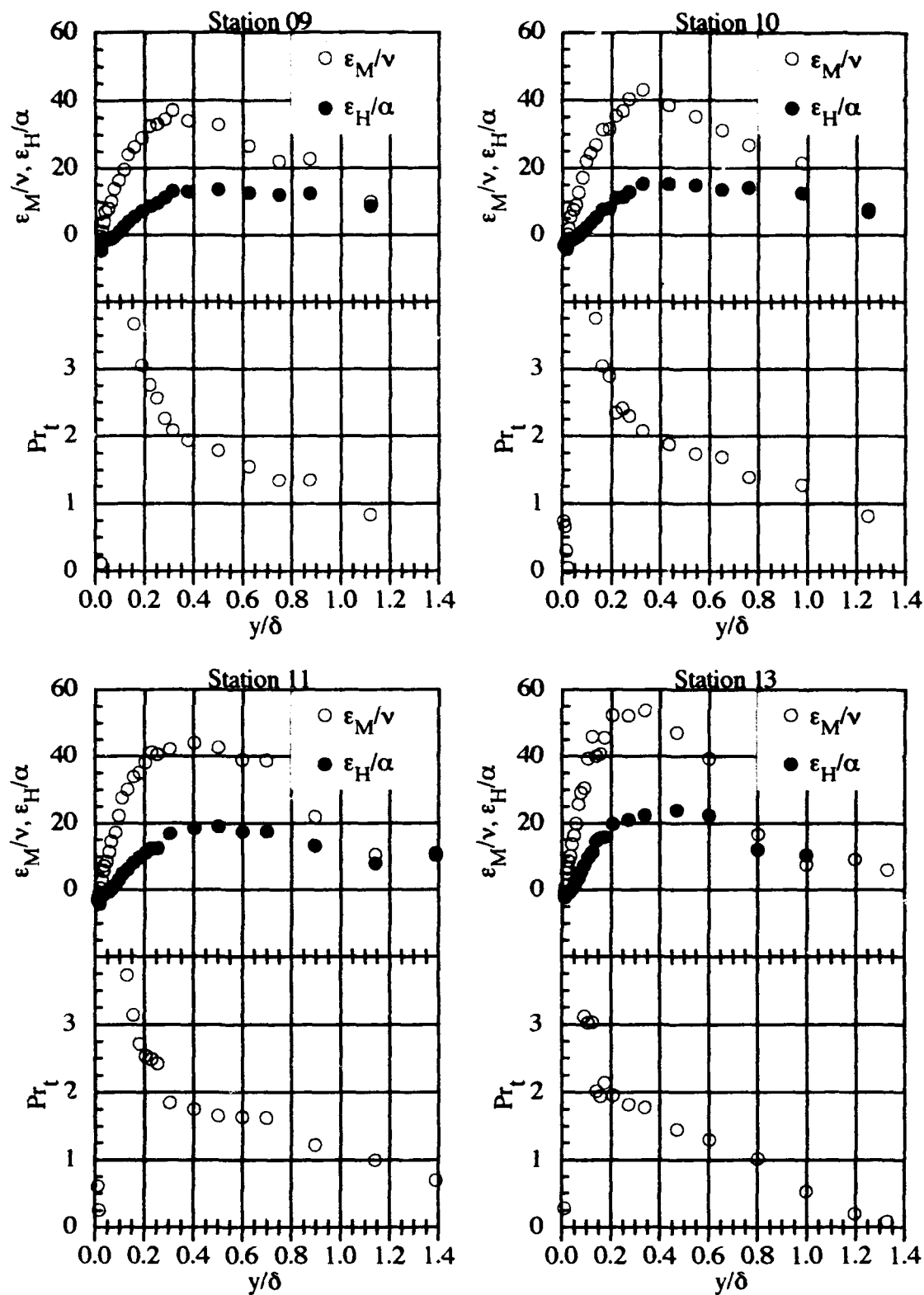


Figure 10 Distribution of eddy viscosity, turbulent thermal diffusivity and turbulent Prandtl number for baseline case (stations 9-11,13).

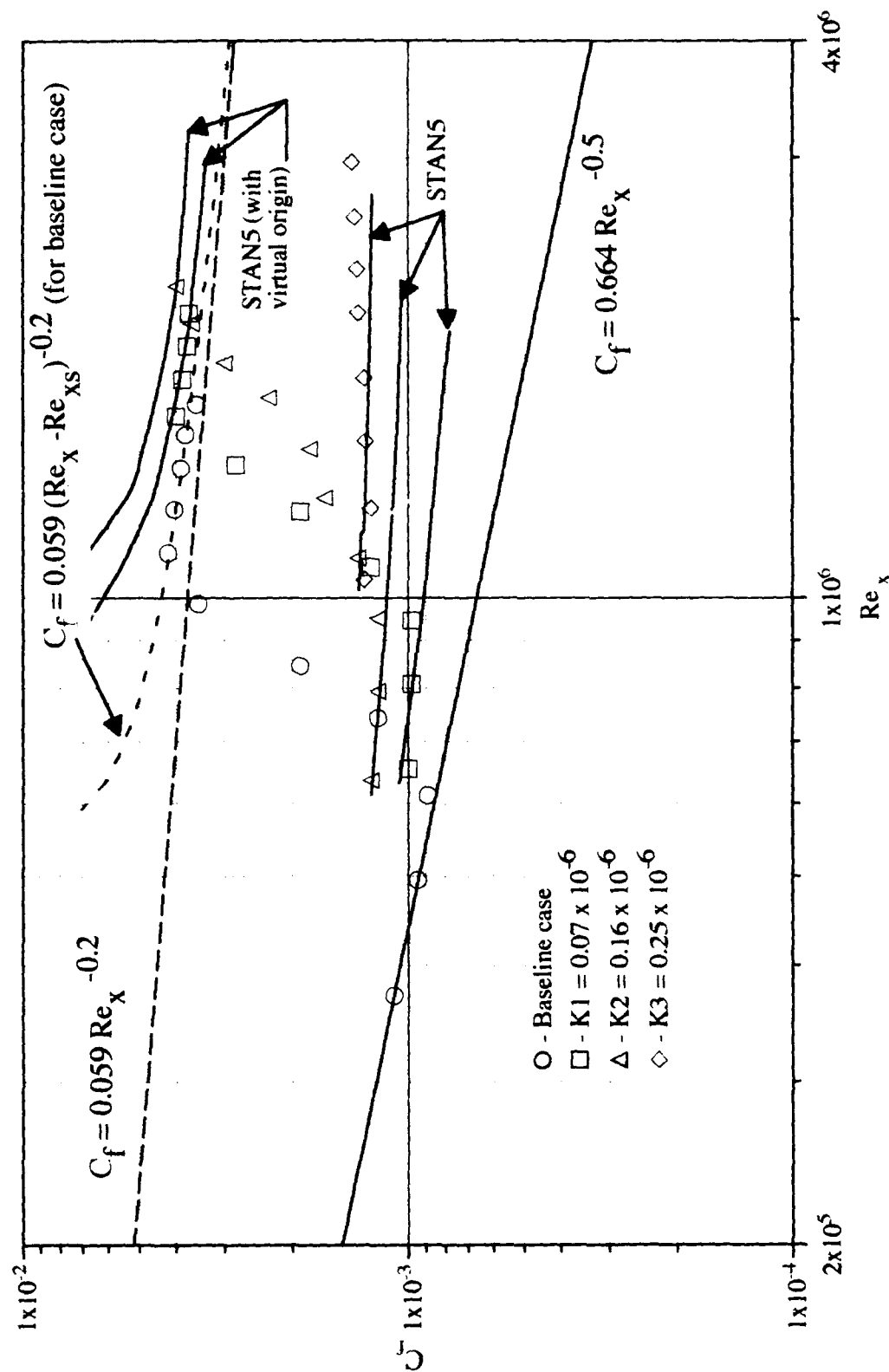


Figure 11 Skin friction coefficient versus Reynolds number for each case.

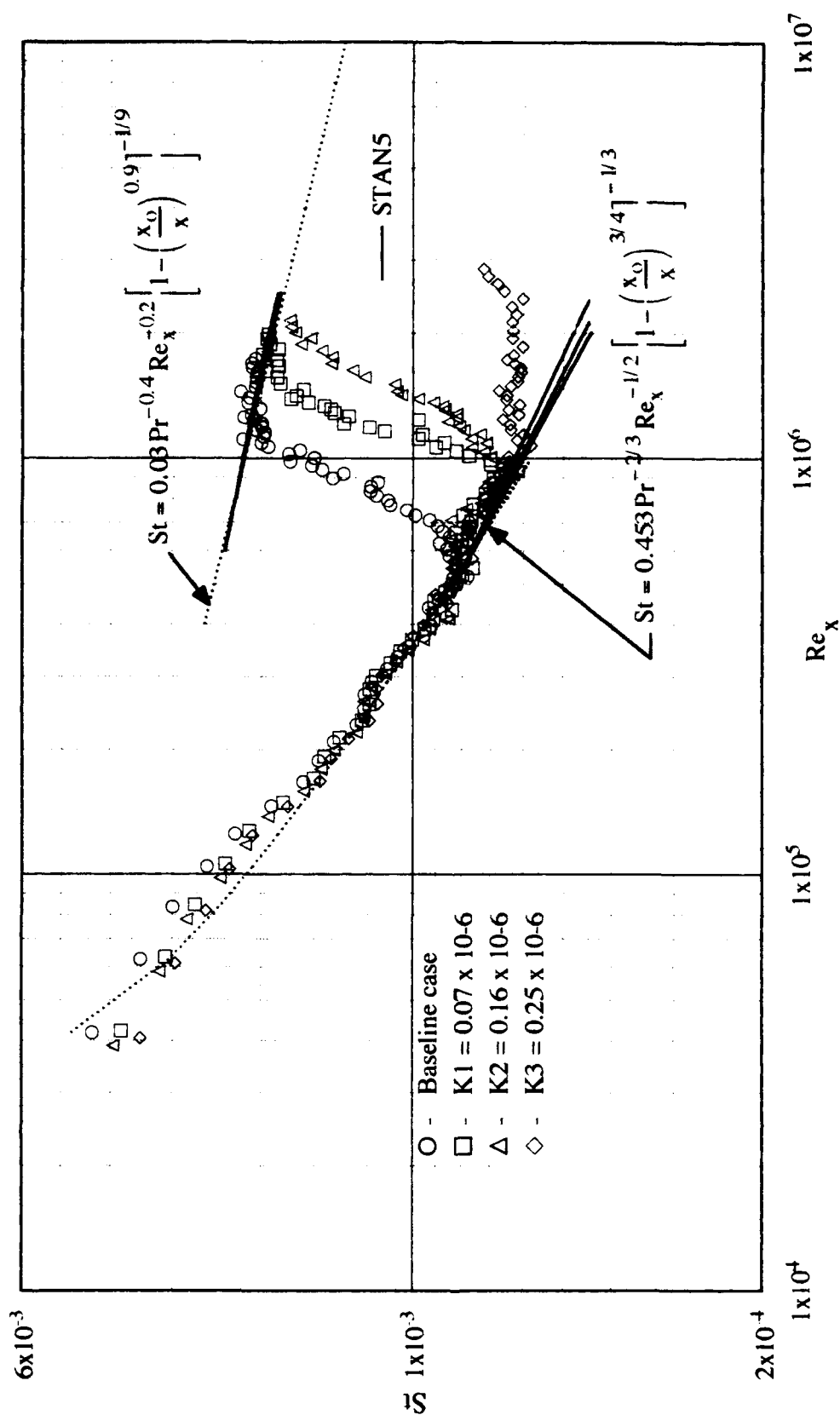


Figure 12 Centerline Stanton number distribution for all cases.

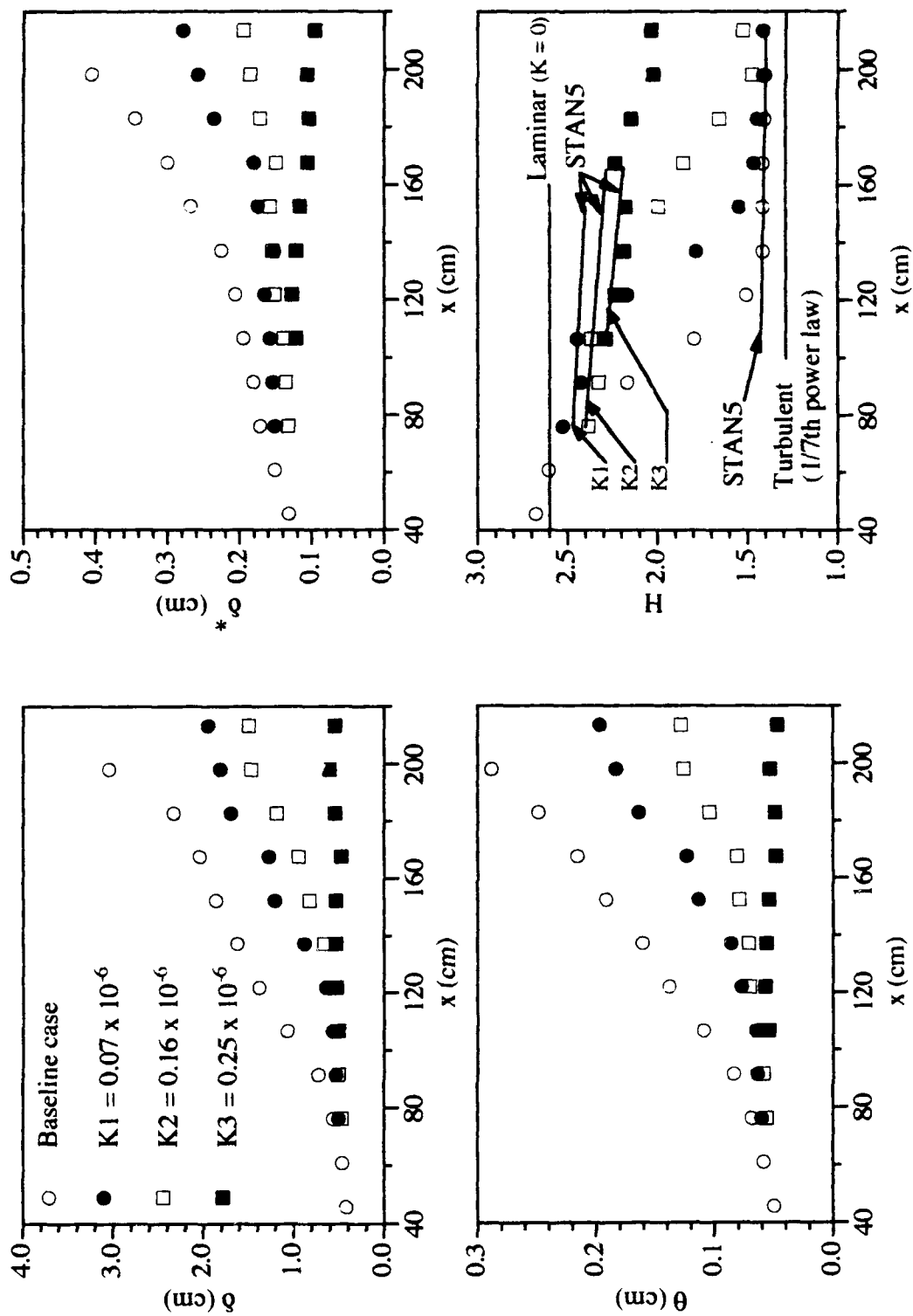


Figure 13 Boundary layer integral parameters for all cases.

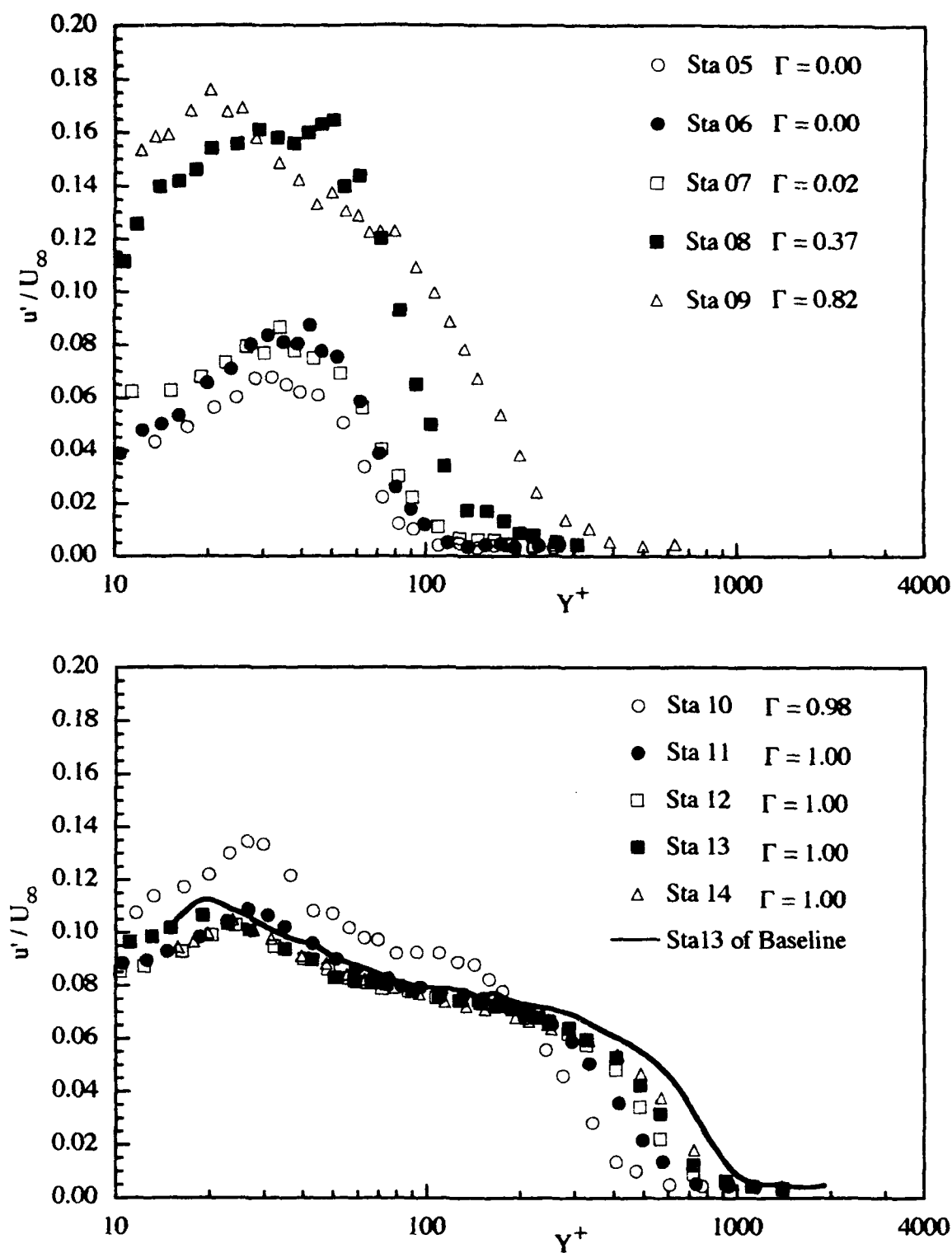


Figure 14 Reynolds normal stress distribution for $K1 = 0.07 \times 10^{-6}$ in wall units.

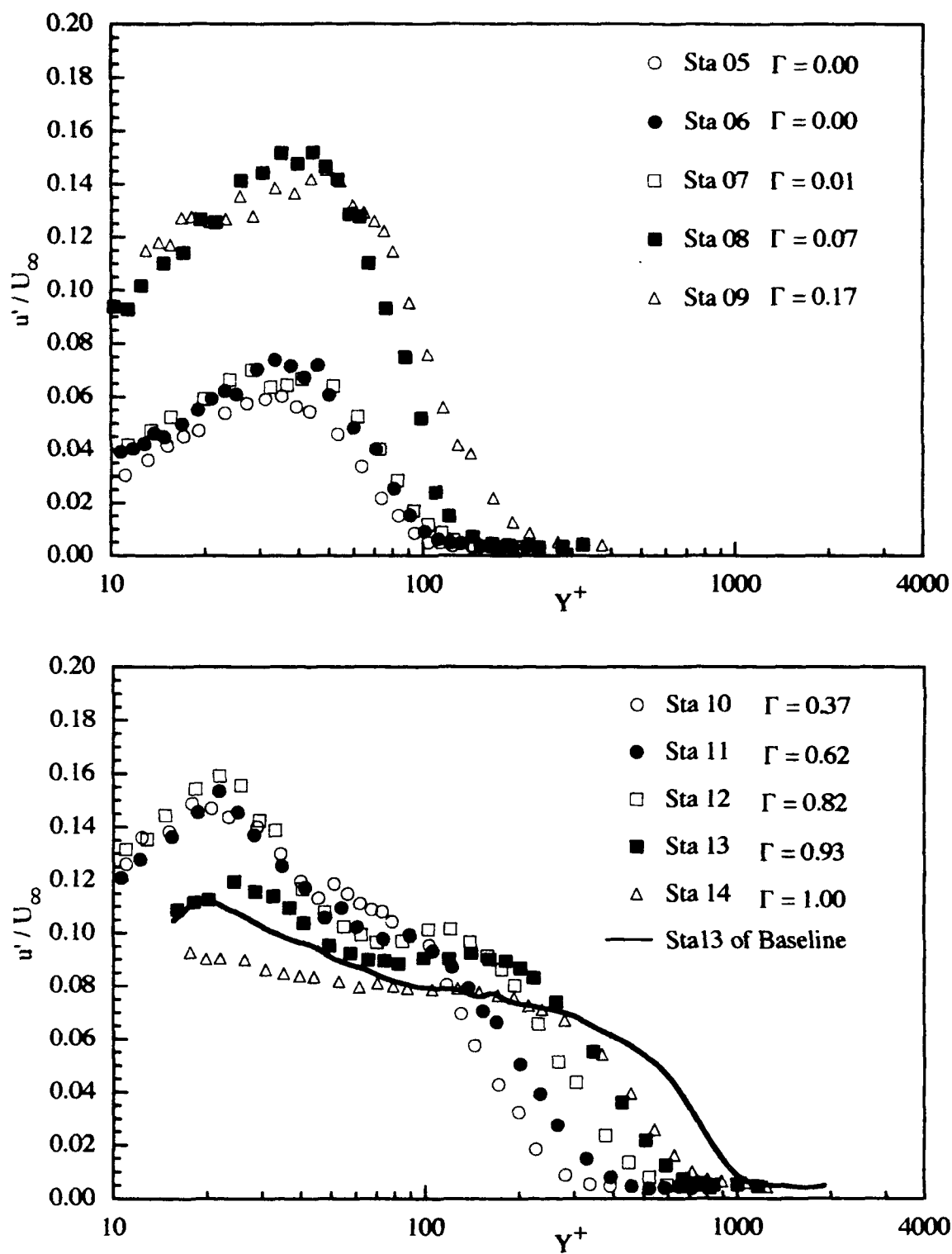


Figure 15 Reynolds normal stress distribution for $K2 = 0.16 \times 10^{-6}$ in wall units.

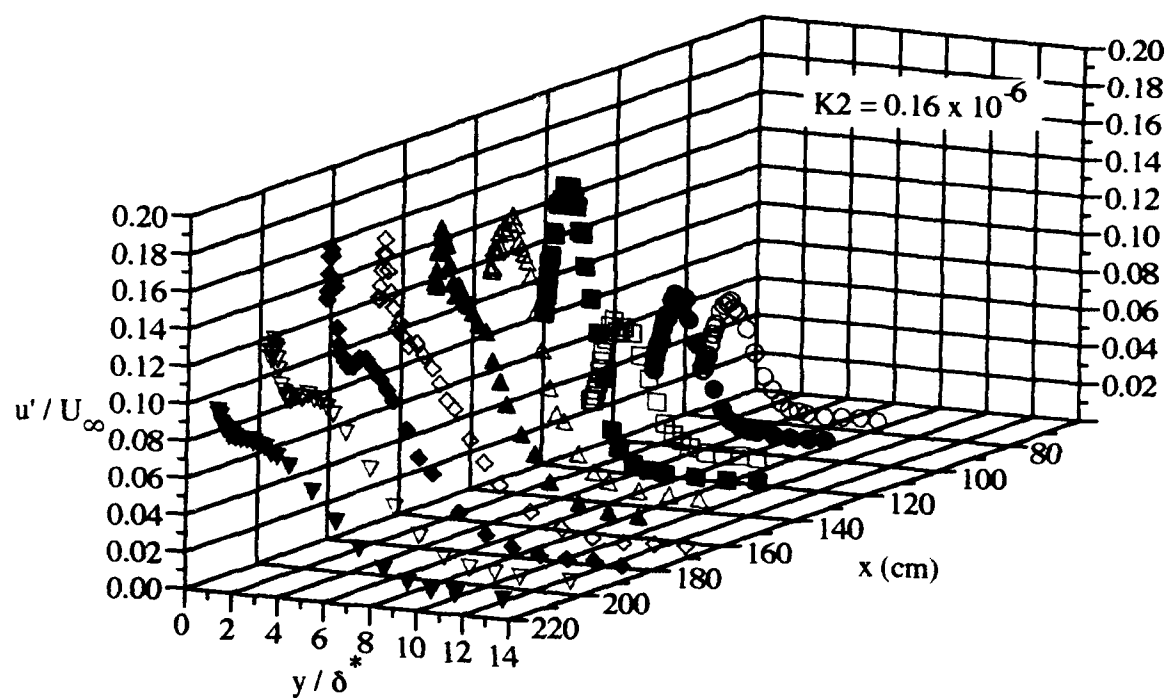
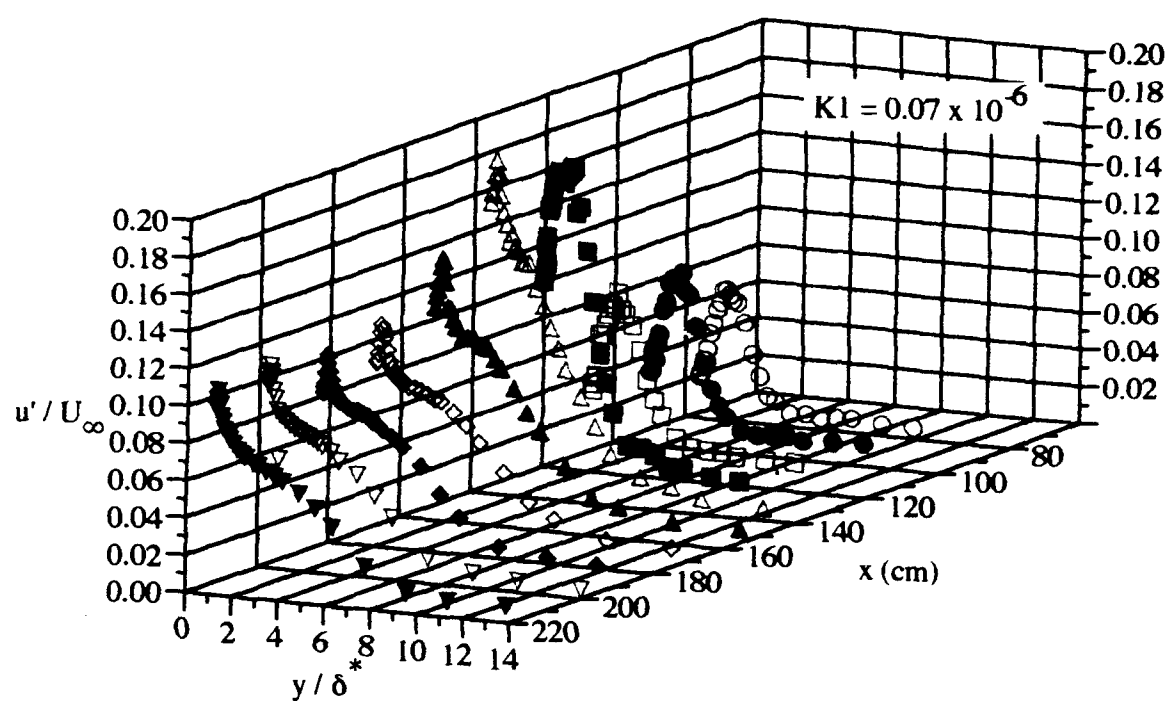


Figure 16 Evolution of streamwise Reynolds normal stress for $K1 = 0.07 \times 10^{-6}$ and $K2 = 0.16 \times 10^{-6}$.

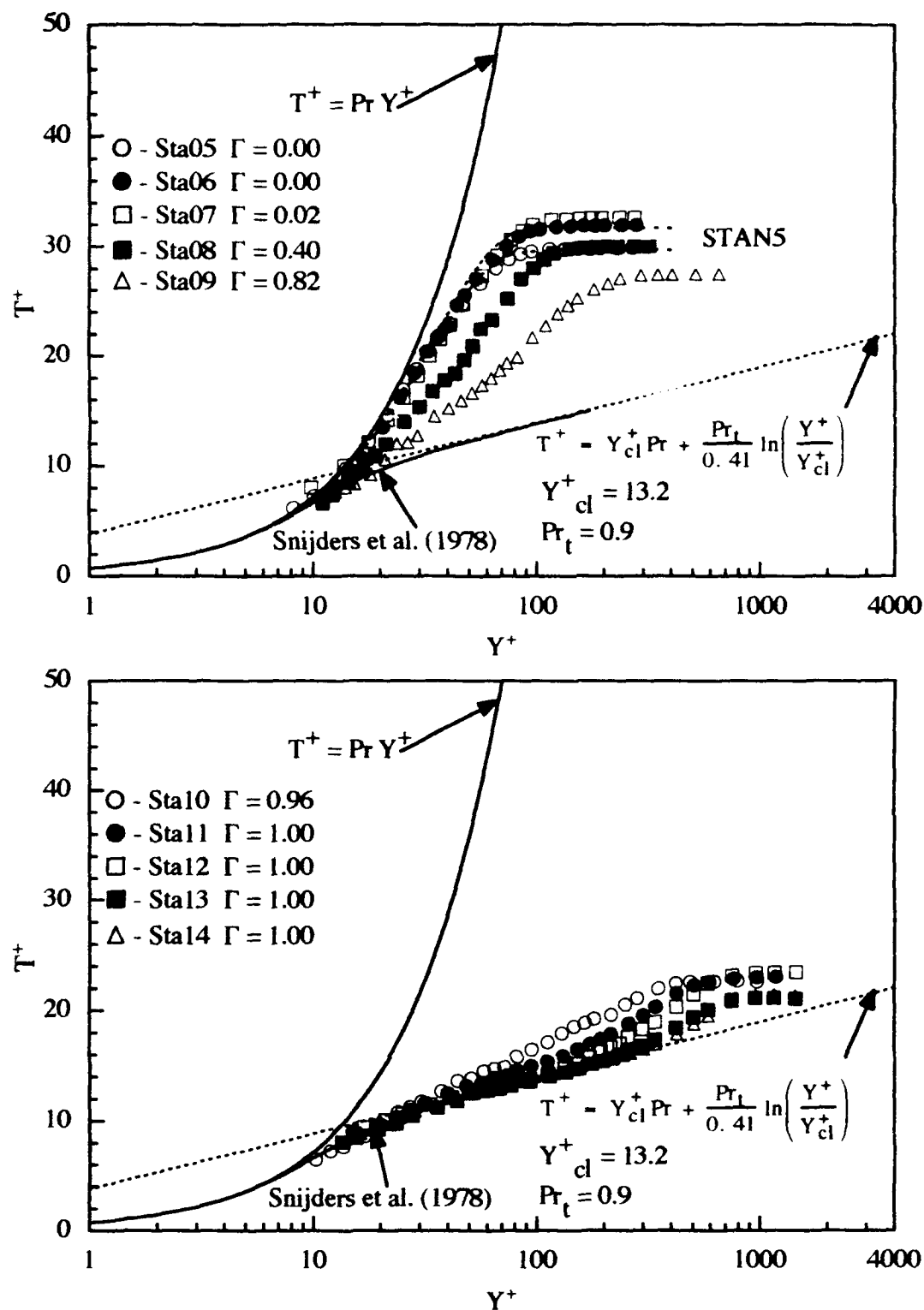


Figure 17 Mean temperature profiles for $K1 = 0.07 \times 10^{-6}$ in wall units.

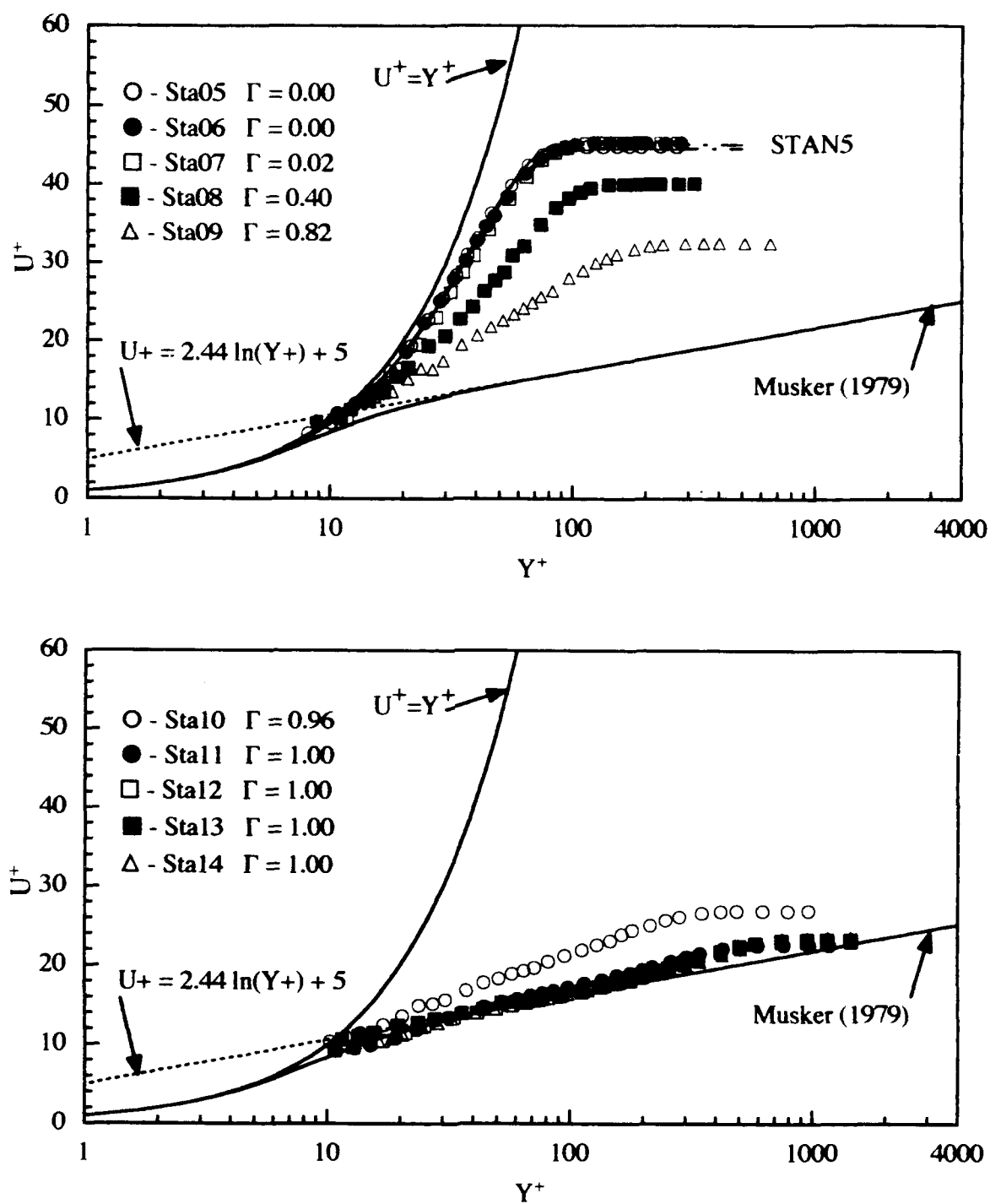


Figure 18 Mean velocity profile for $K1 = 0.07 \times 10^{-6}$ in wall units.

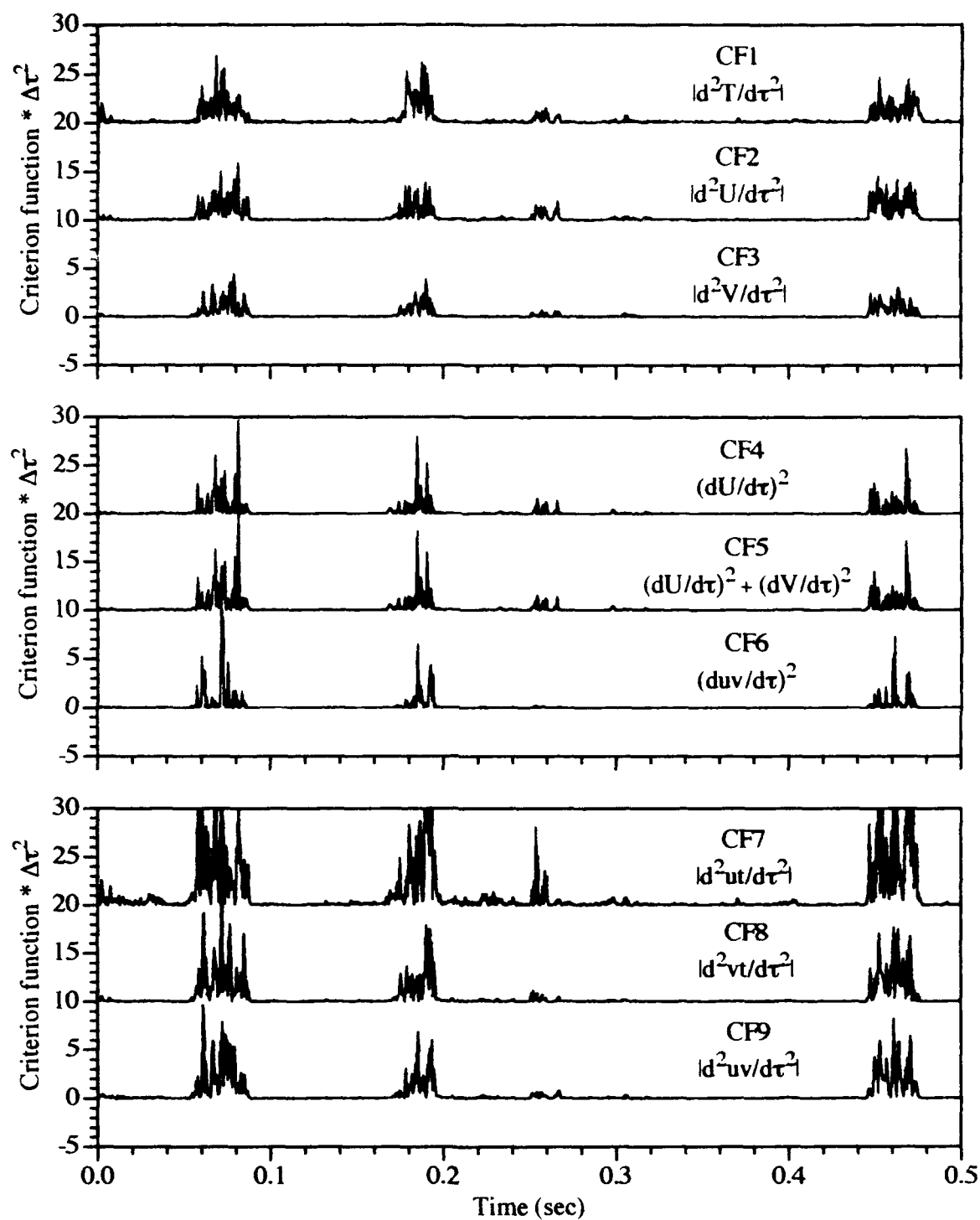


Figure 19 Corresponding criterion functions for $\Gamma = 0.5$, $y/\delta^* = 1.1$ (baseline case).

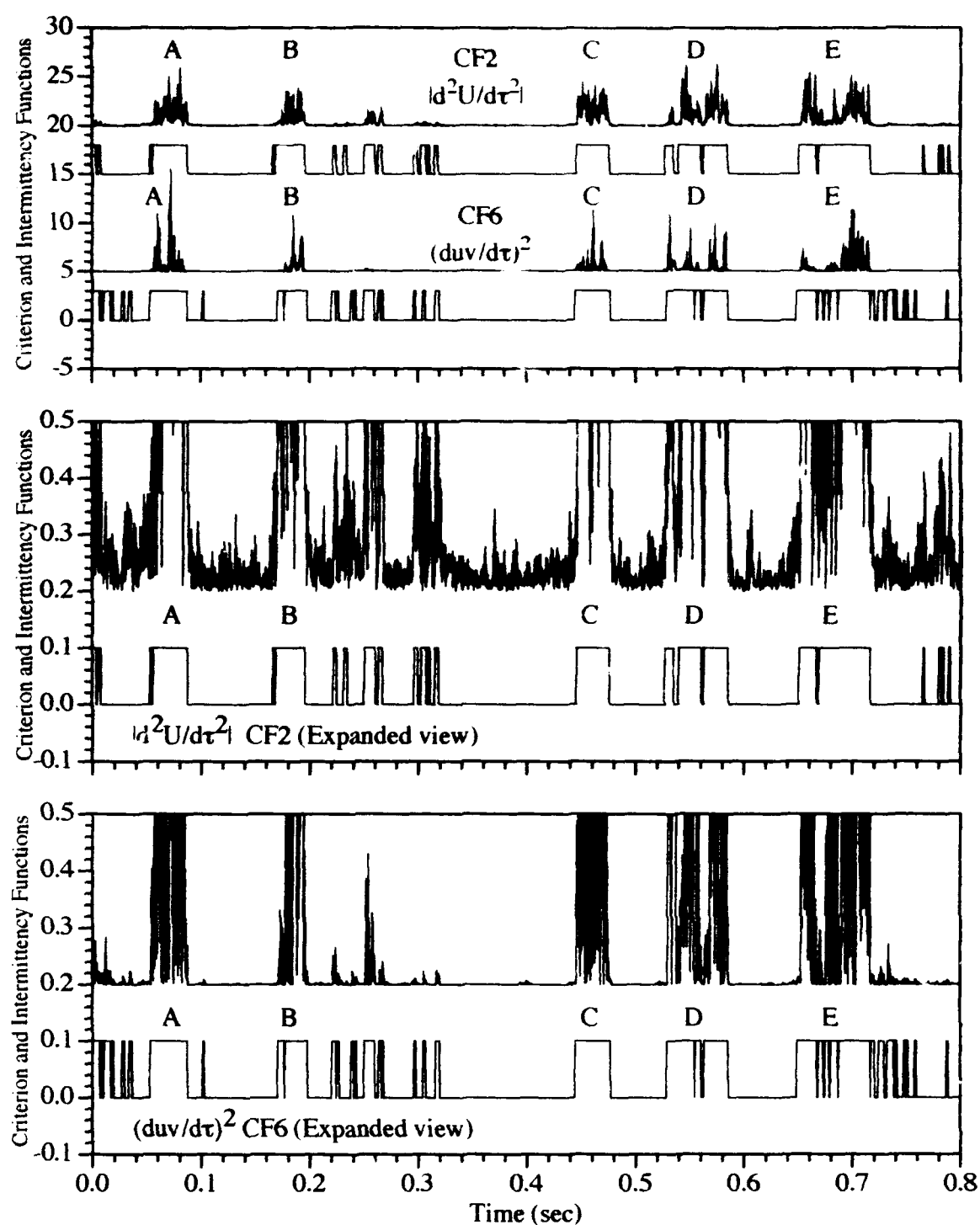


Figure 20 Comparison of two criterion functions and corresponding intermittency functions for $\Gamma = 0.5$, $y/\delta^* = 1.1$ (baseline case).

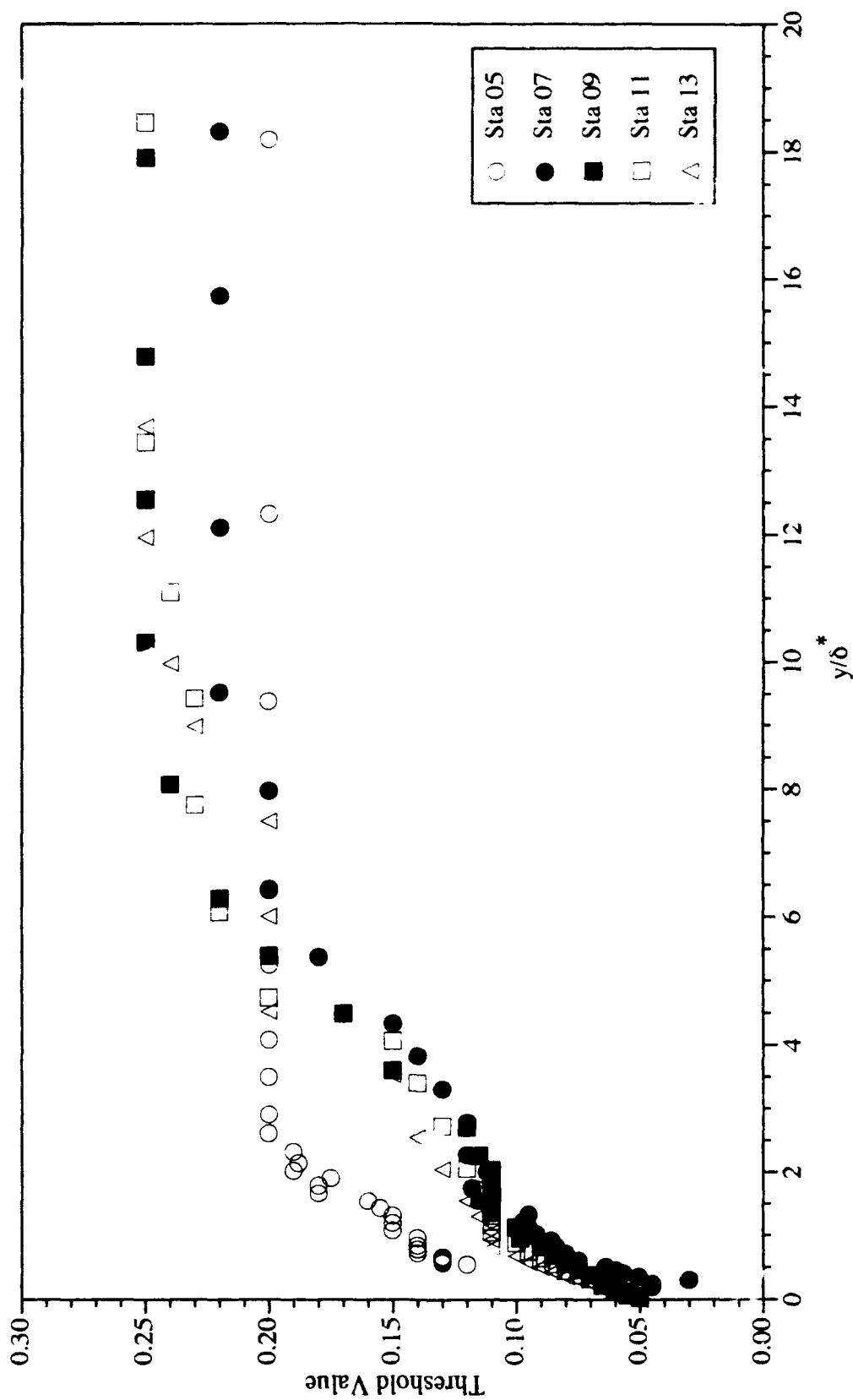


Figure 21 Distribution of threshold value for several stations of the baseline case using $|d^2(1/d\tau^2)|$ (CF2).

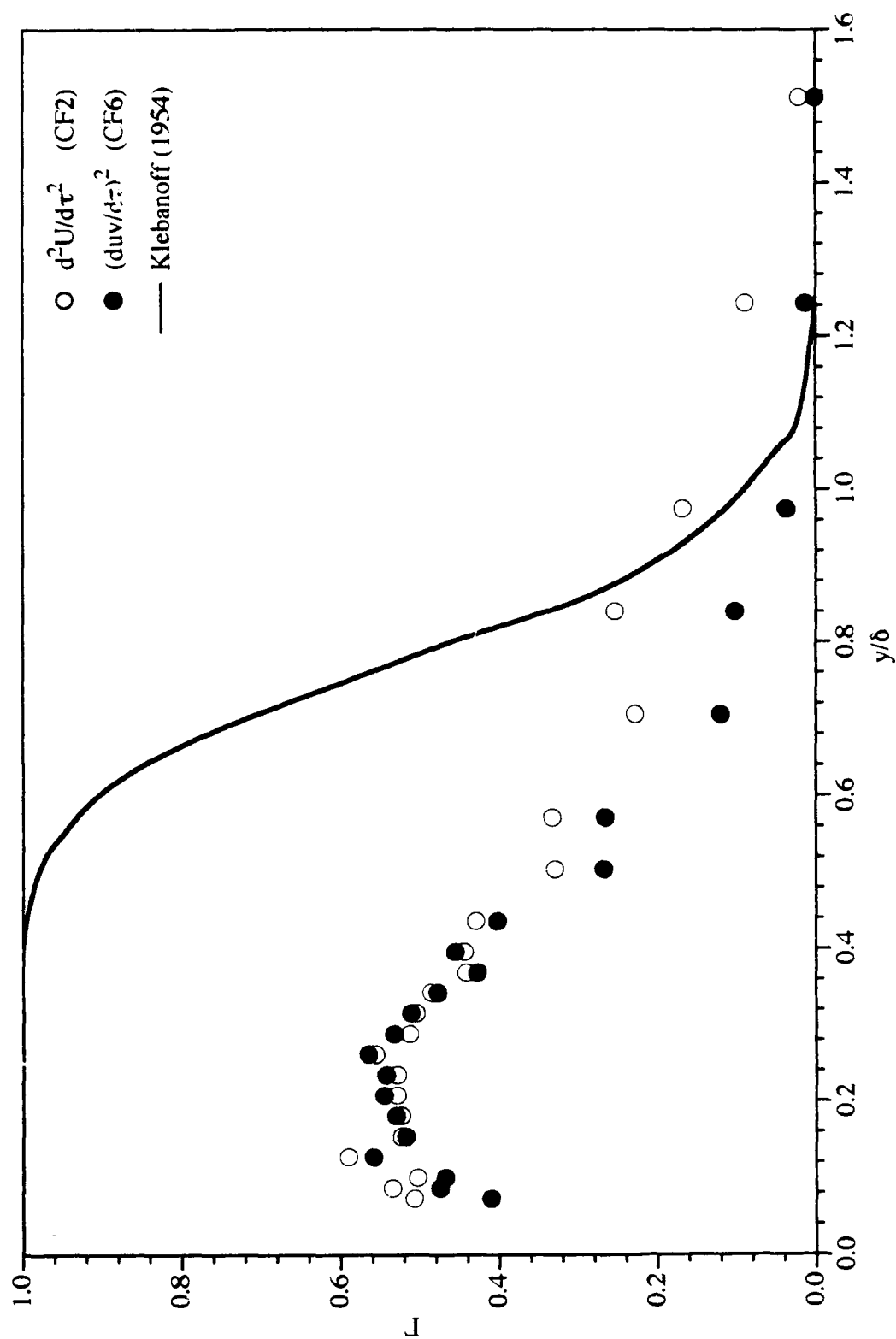


Figure 22 Intermittency distribution through the boundary layer for different criterion functions (station 06, baseline case).

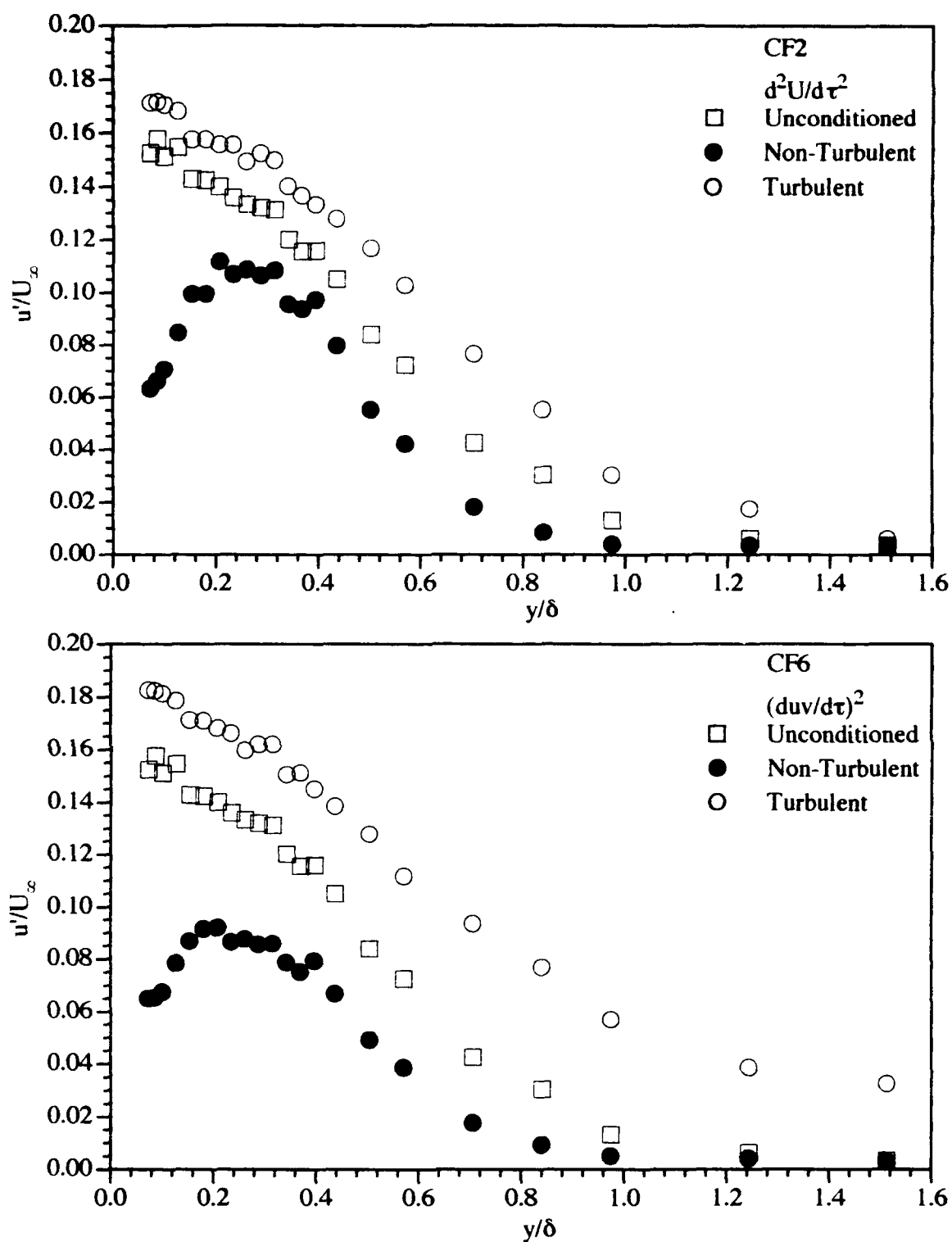


Figure 23 Comparison of streamwise Reynolds normal stress for different criterion functions (station 06, $\Gamma = 0.5$, baseline case).

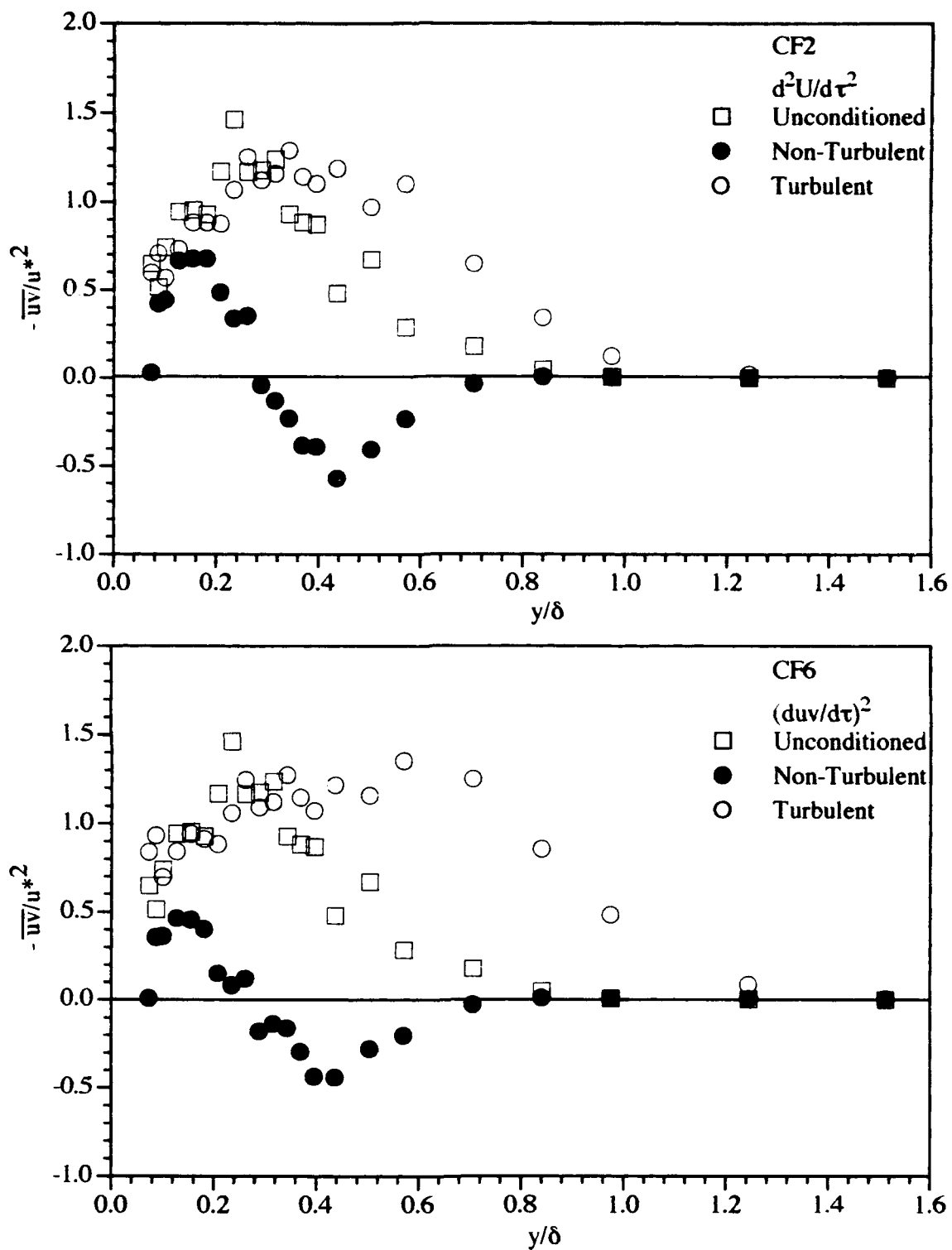
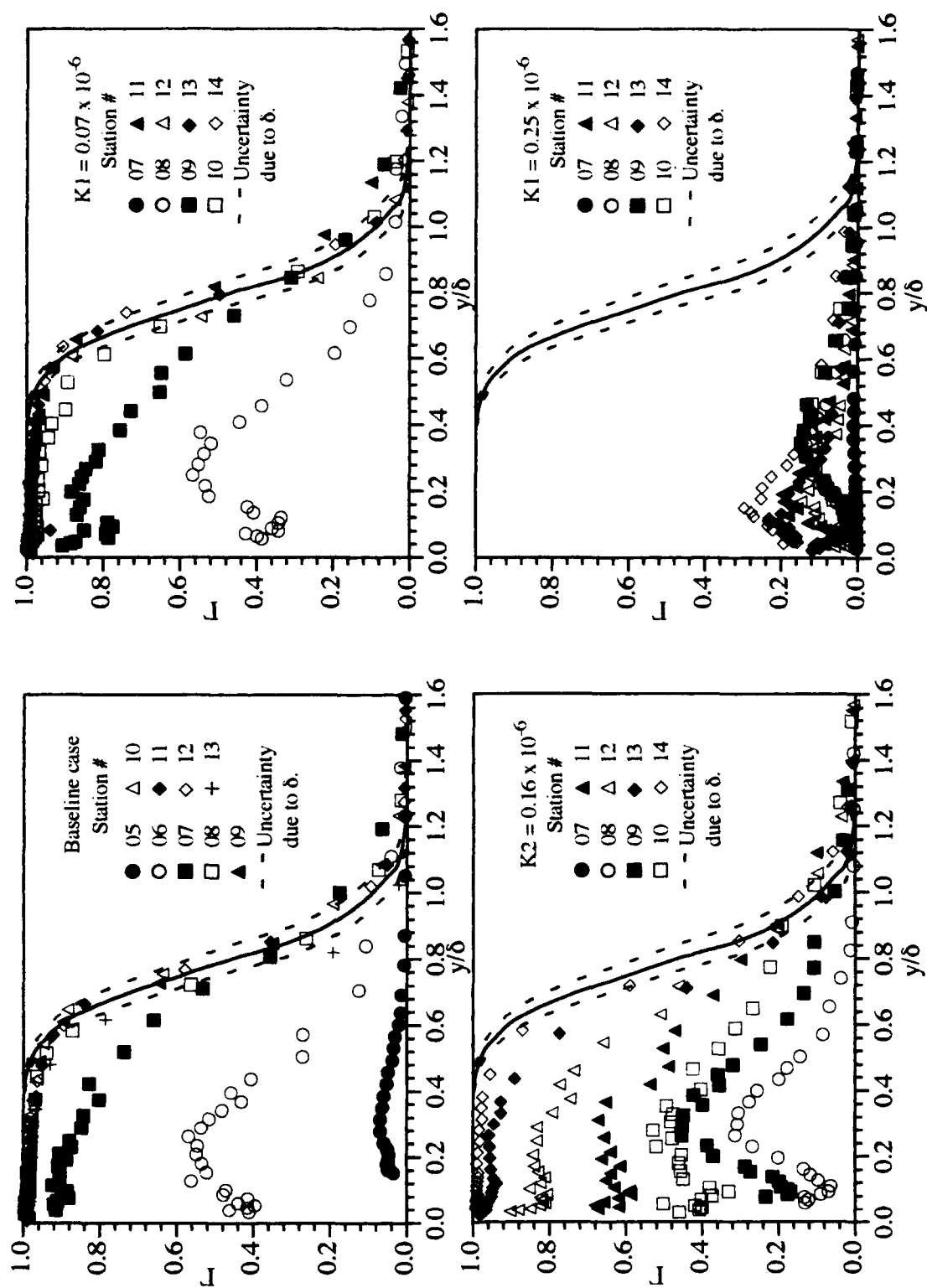


Figure 24 Comparison of Reynolds shear stress for different criterion functions (station 06, $\Gamma = 0.5$, baseline case).

Figure 25 Intermittency distribution through boundary layer using $(duv/d\tau)^2$.

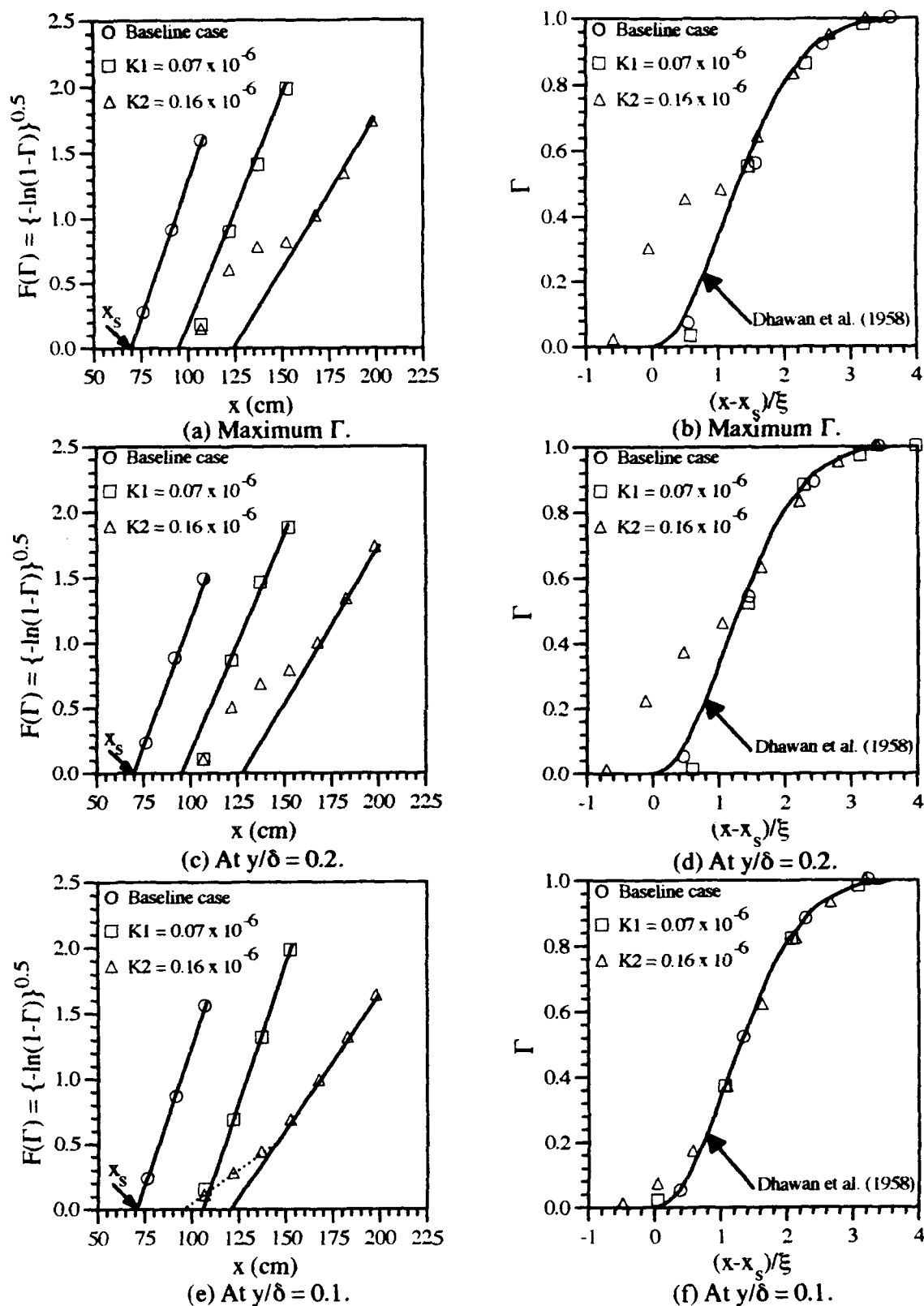


Figure 26 Determination of x_s and corresponding representative near-wall intermittency in Γ versus x coordinates using the value of Γ at different y/δ locations as the representative intermittency.

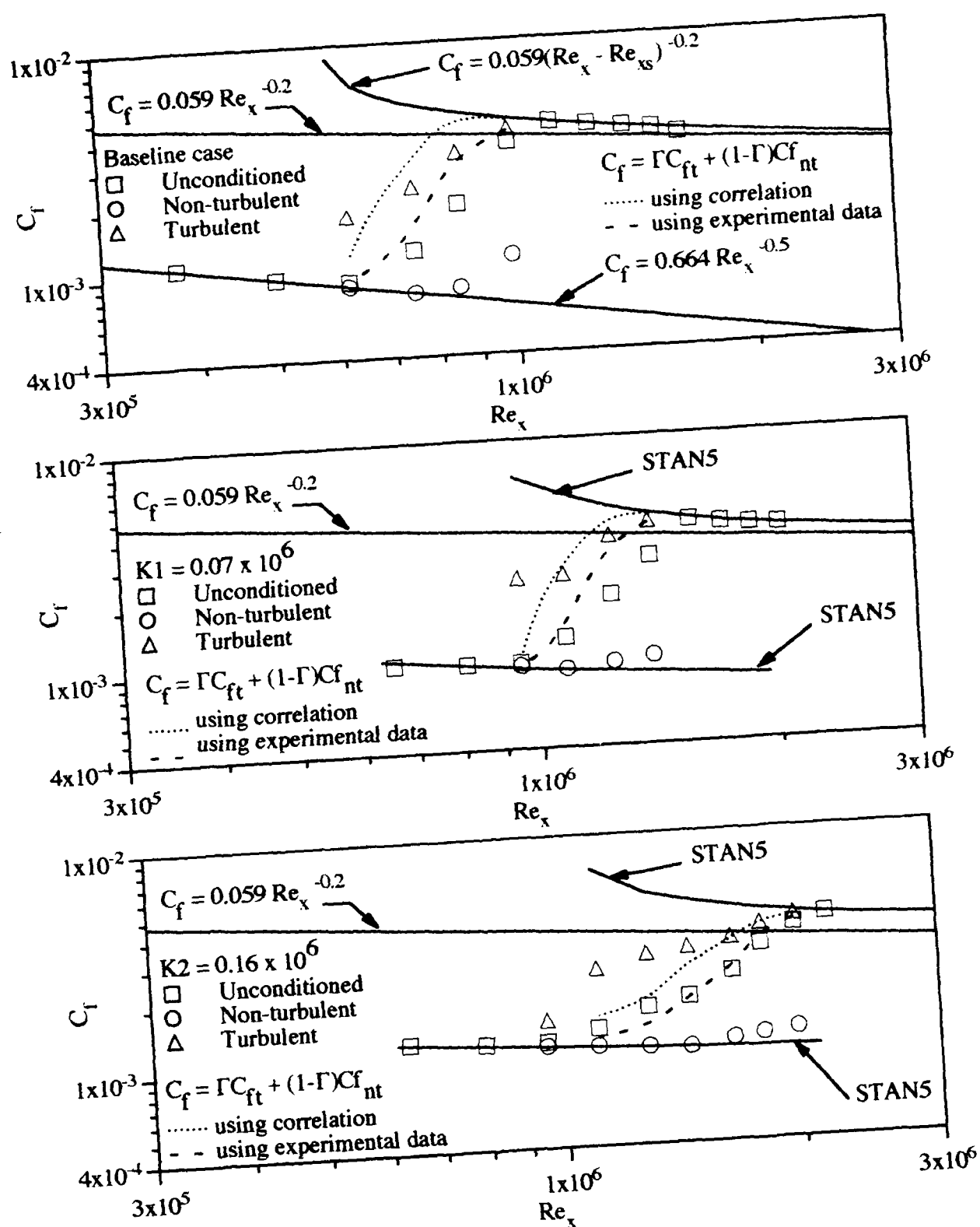


Figure 27 Conditionally sampled skin friction coefficient.

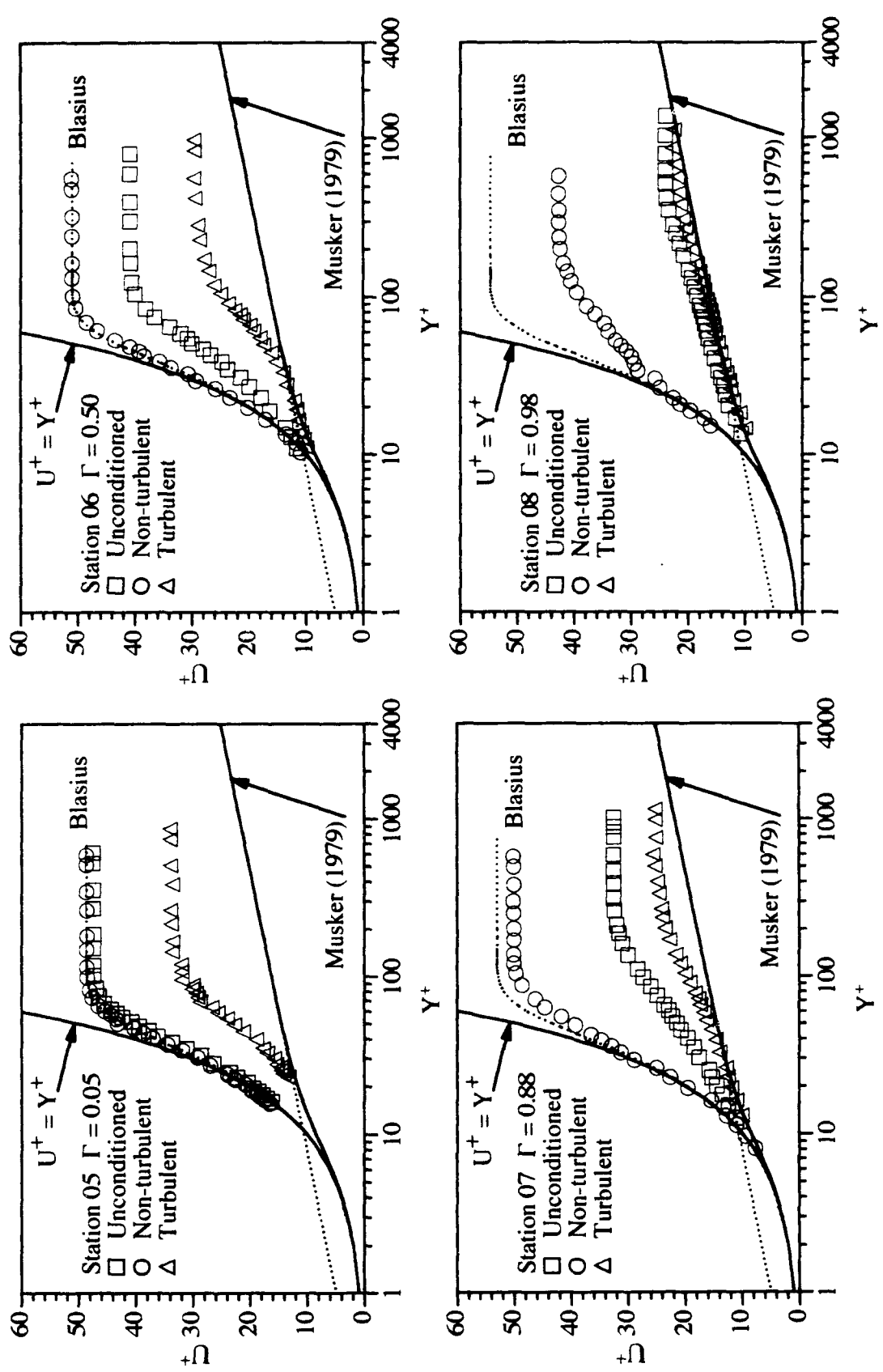


Figure 28 Conditionally sampled mean velocity profiles for the baseline case (in wall units).

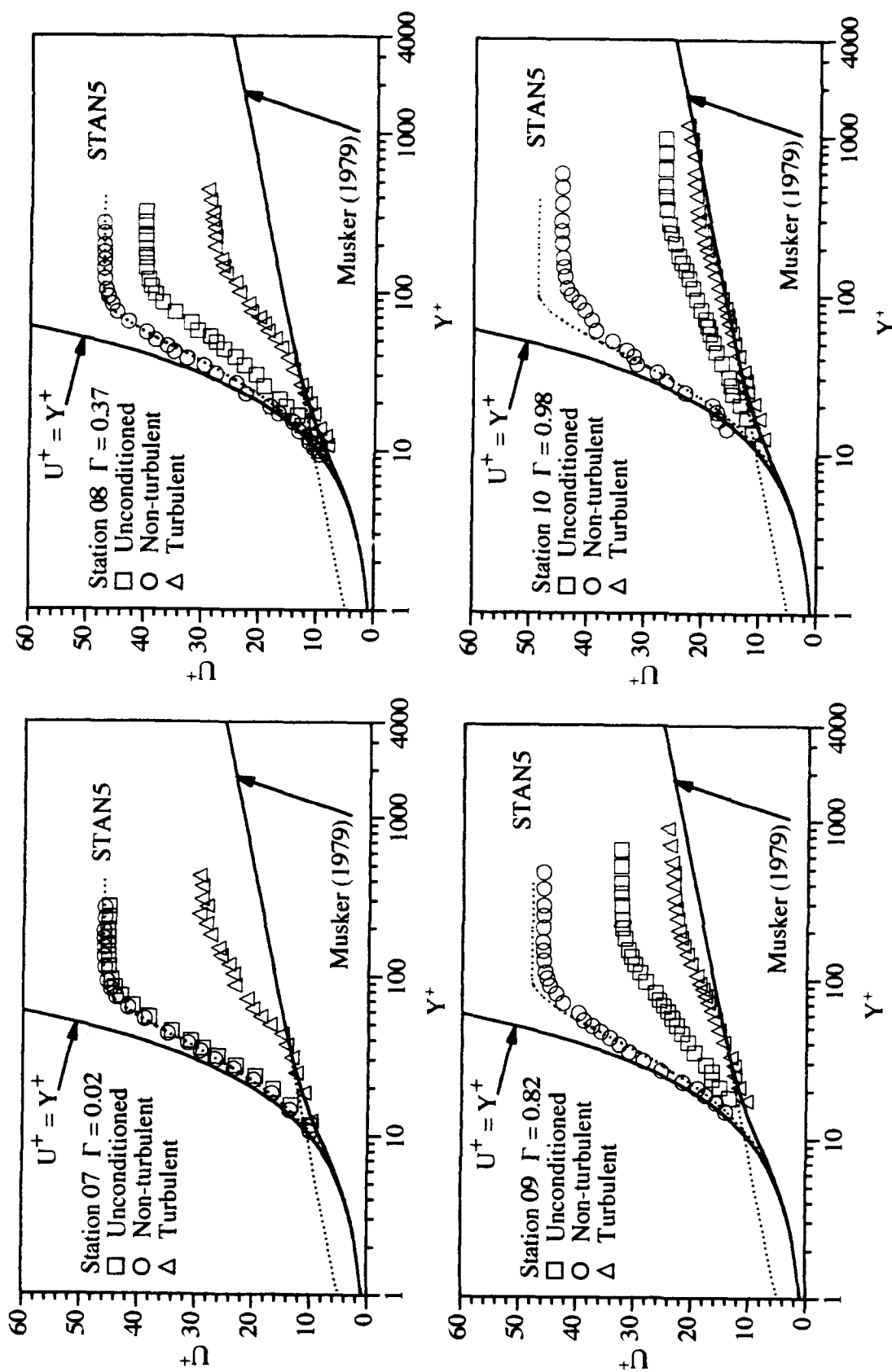


Figure 29 Conditionally sampled mean velocity profiles for the K1 case (in wall units).

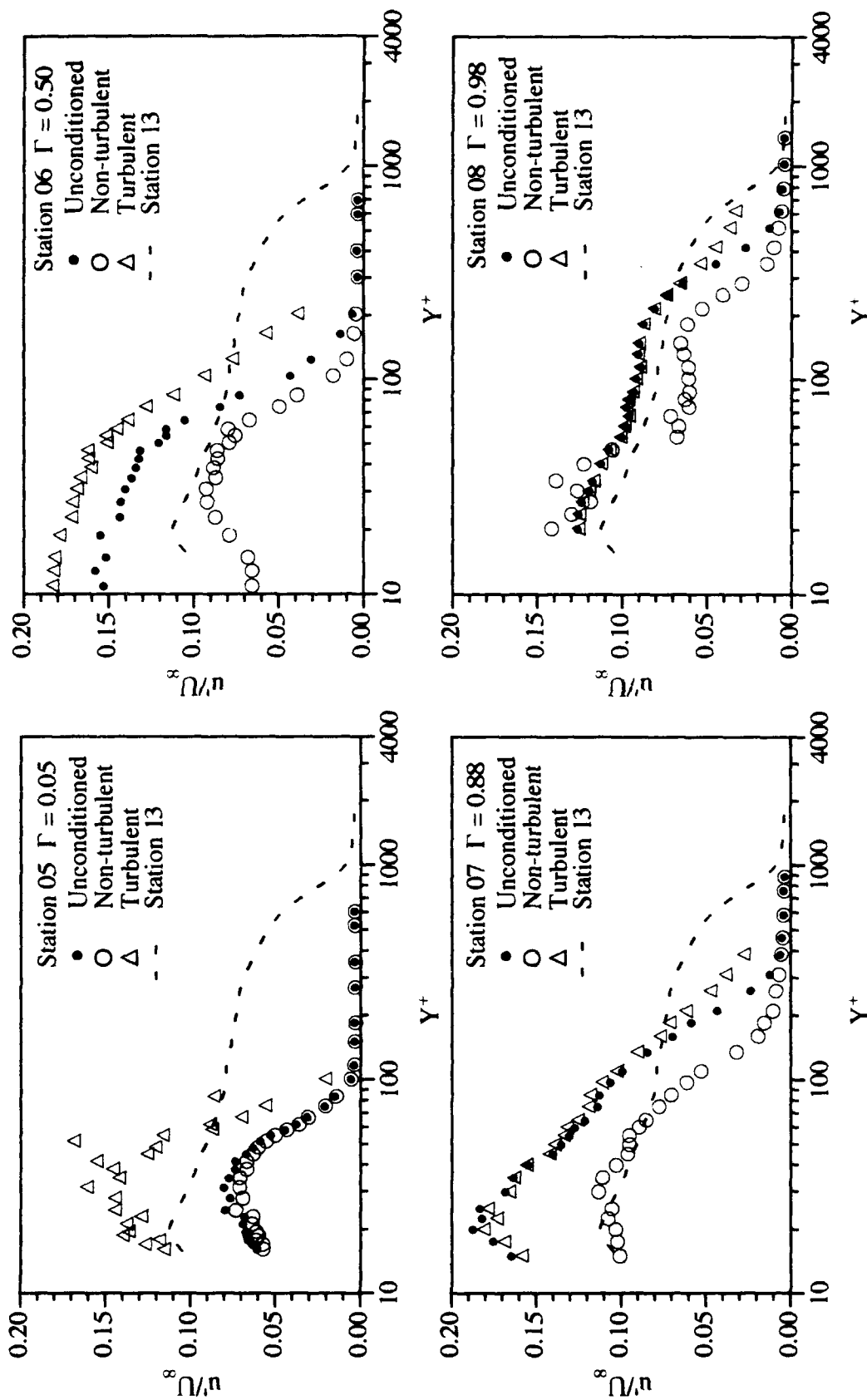


Figure 30 Conditionally sampled streamwise Reynolds normal stress for the baseline case (in wall units)
(Note: data points in the turbulent portion when $\Gamma < 0.005$ are omitted).

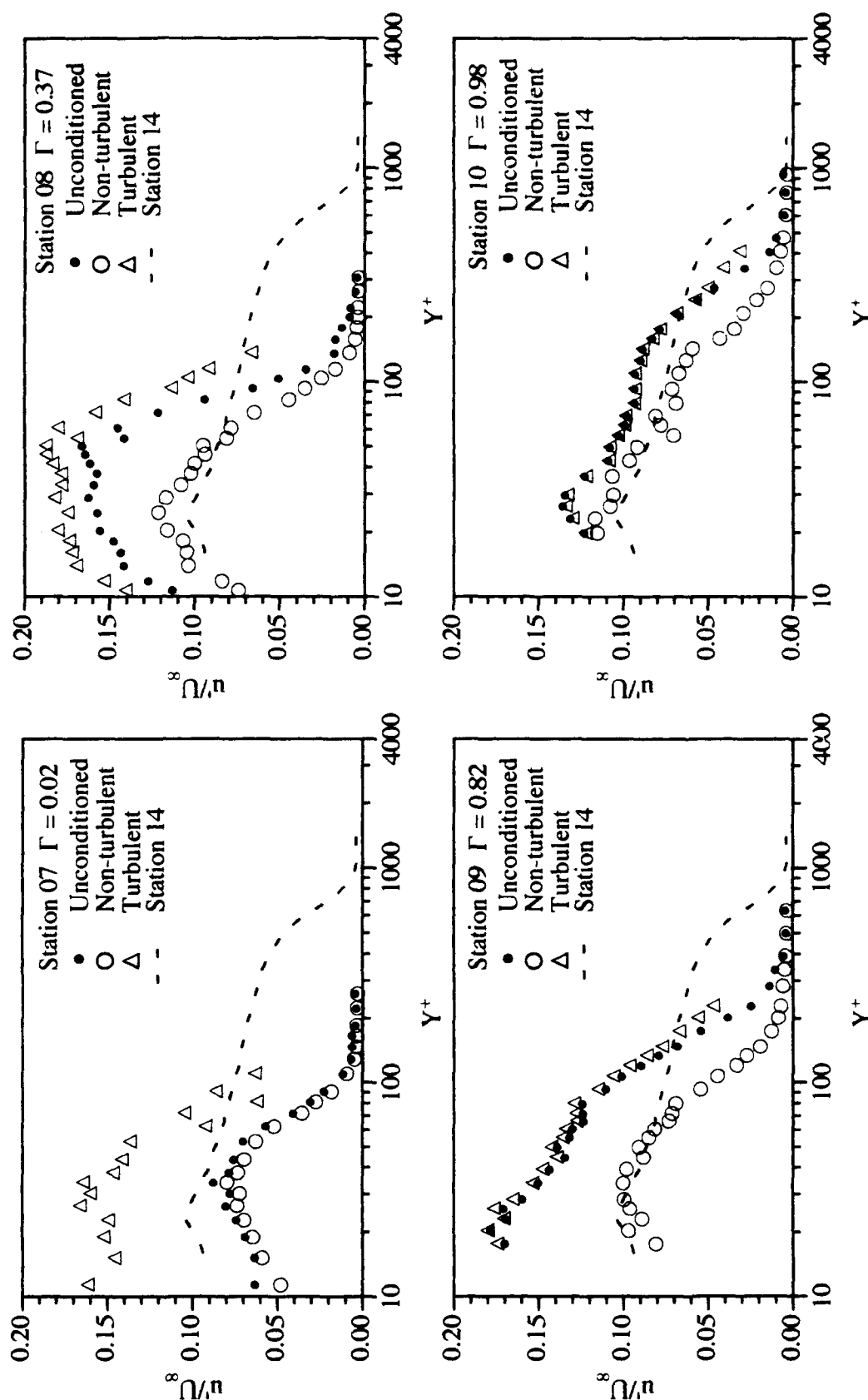


Figure 31 Conditionally sampled streamwise Reynolds normal stress for the K1 case (in wall units)
(Note: data points in the turbulent portion when $\Gamma < 0.005$ are omitted).

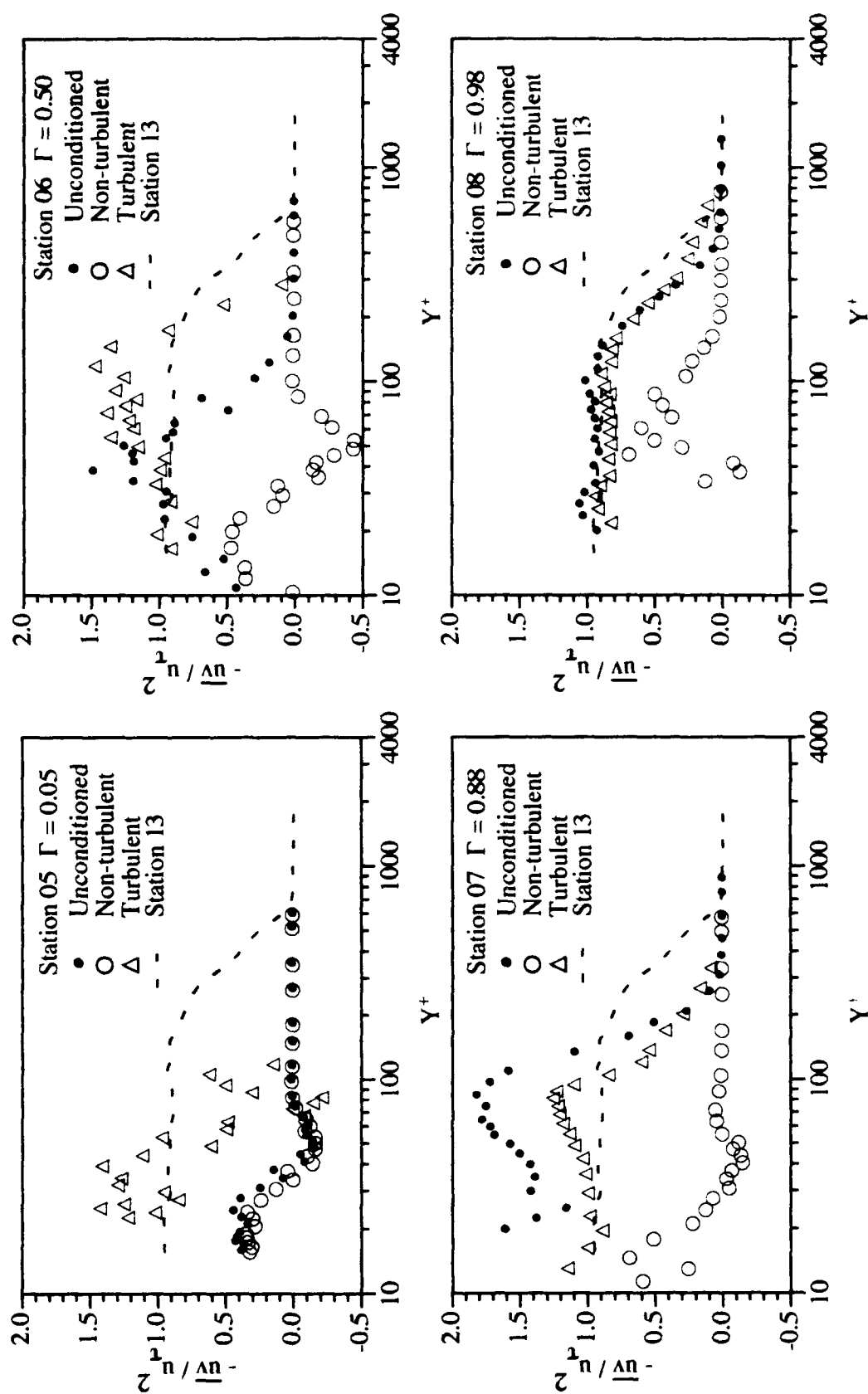


Figure 32 Conditionally sampled Reynolds shear stress for the baseline case (normalized by individual C_f of each portion)
(Note: data points in the turbulent portion when $\Gamma < 0.005$ are omitted).

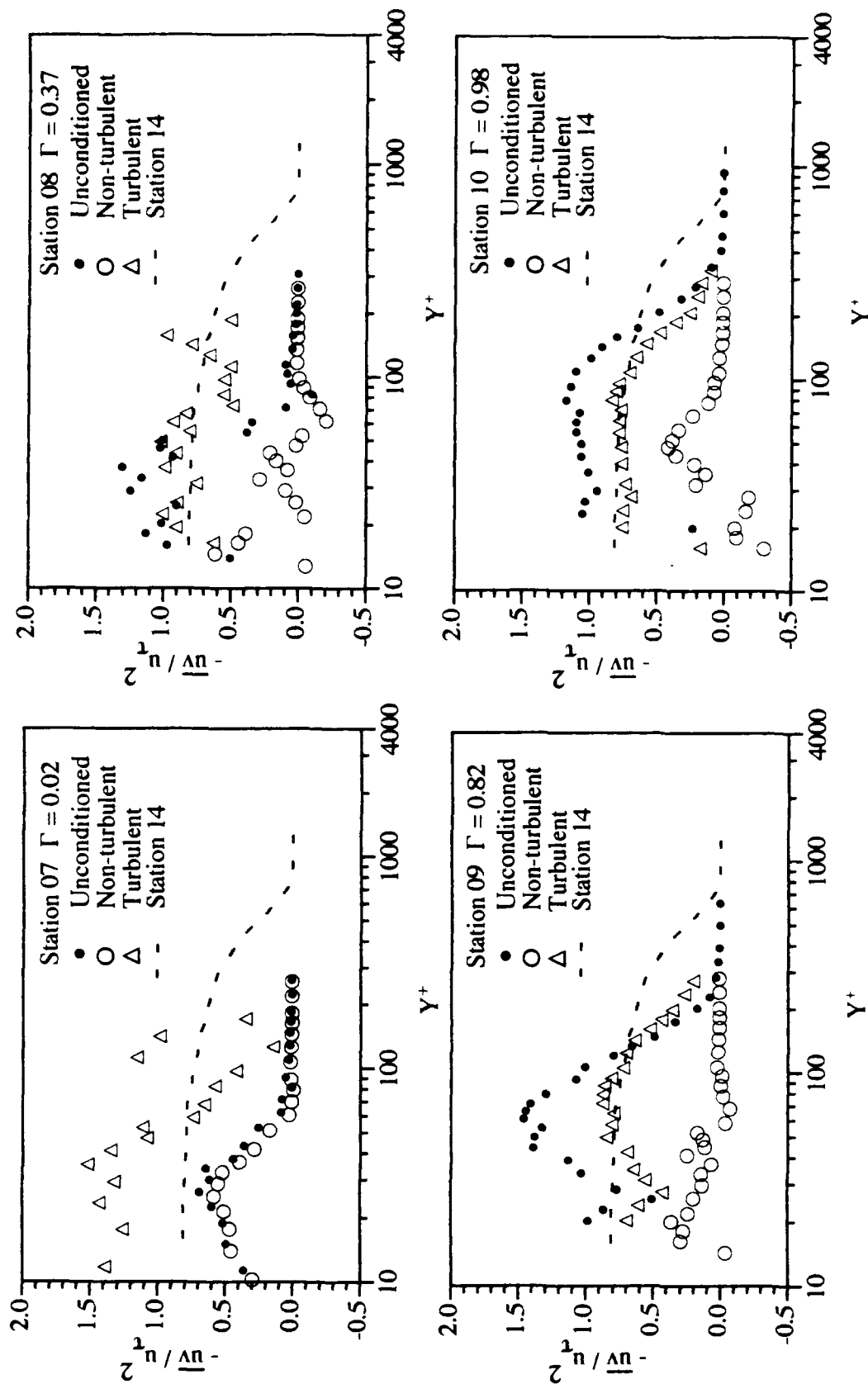


Figure 33 Conditionally sampled Reynolds shear stress for the K1 case (normalized by individual C_f of each portion)
(Note: data points in the turbulent portion when $\Gamma < 0.005$ are omitted).

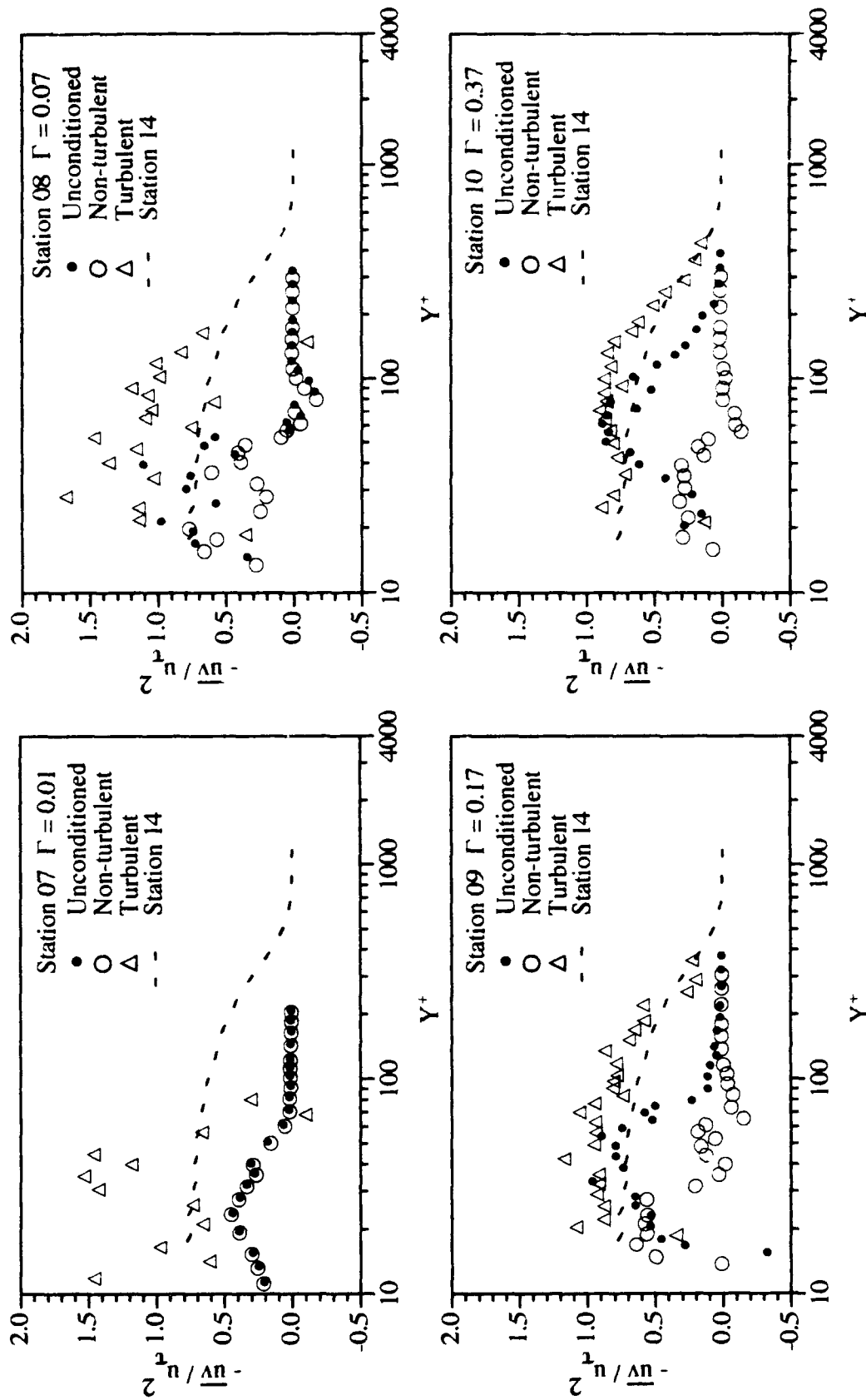


Figure 34 Conditionally sampled Reynolds shear stress for the K2 case, stations 07-10 (normalized by individual C_f of each portion)
(Note: data points in the turbulent portion when $\Gamma < 0.005$ are omitted).

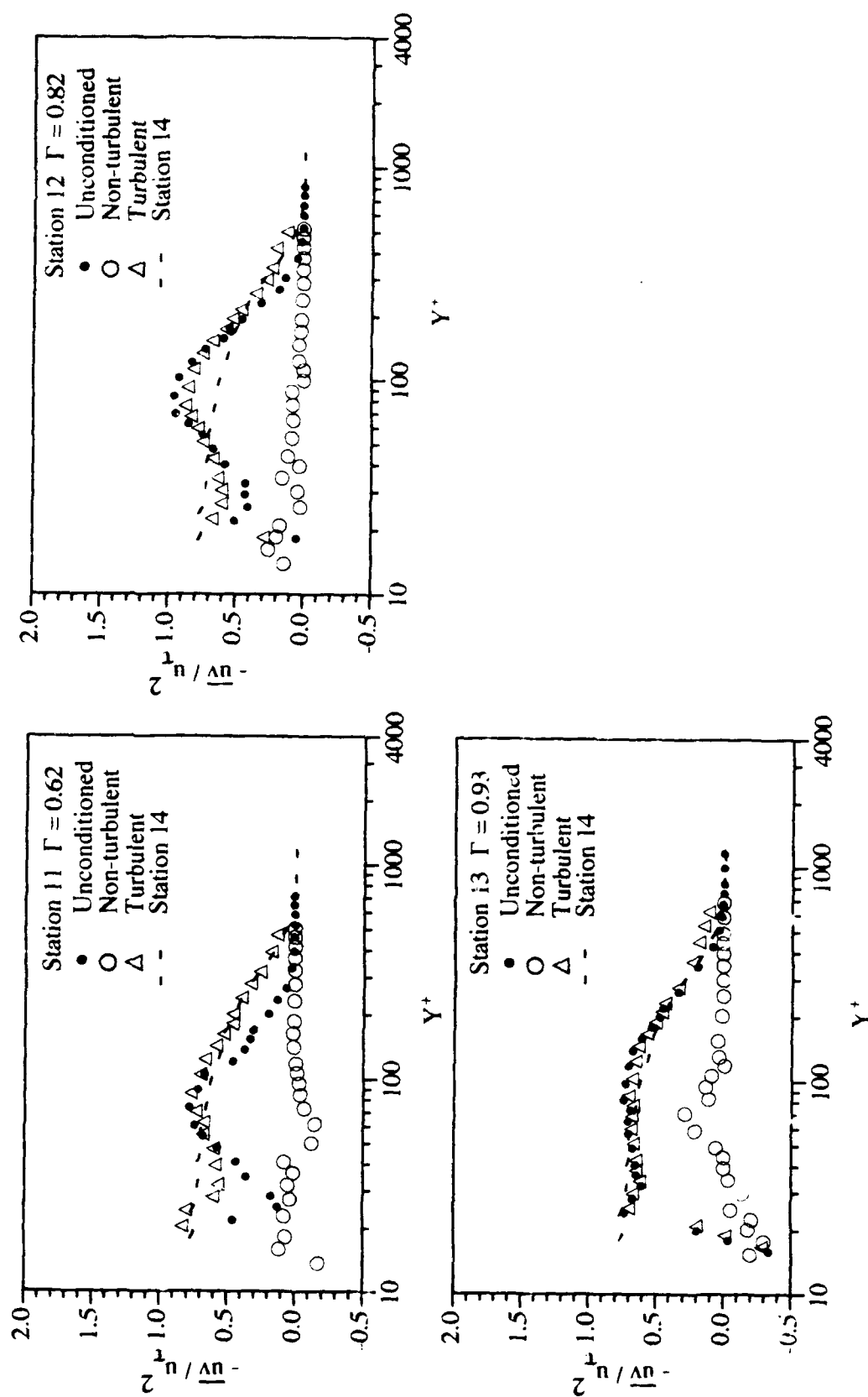


Figure 34 (Continued) (stations 11-13 normalized by individual C_f of each portion)
(Note: data points in the turbulent portion when $\Gamma < 0.005$ are omitted).

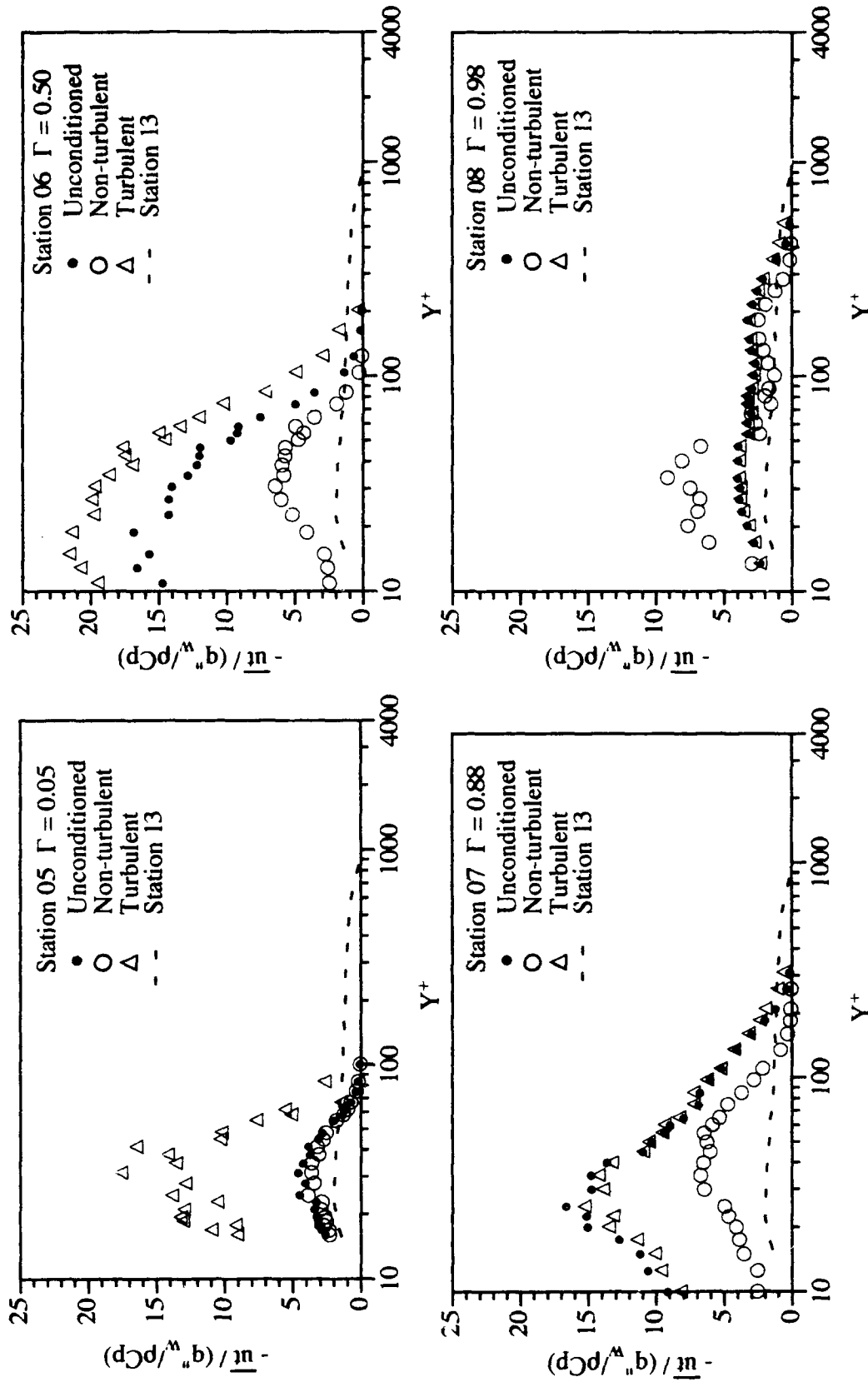


Figure 35 Conditionally sampled Reynolds streamwise heat flux for the baseline case (in wall units)
(Note: data points in the turbulent portion when $\Gamma < 0.005$ are omitted).

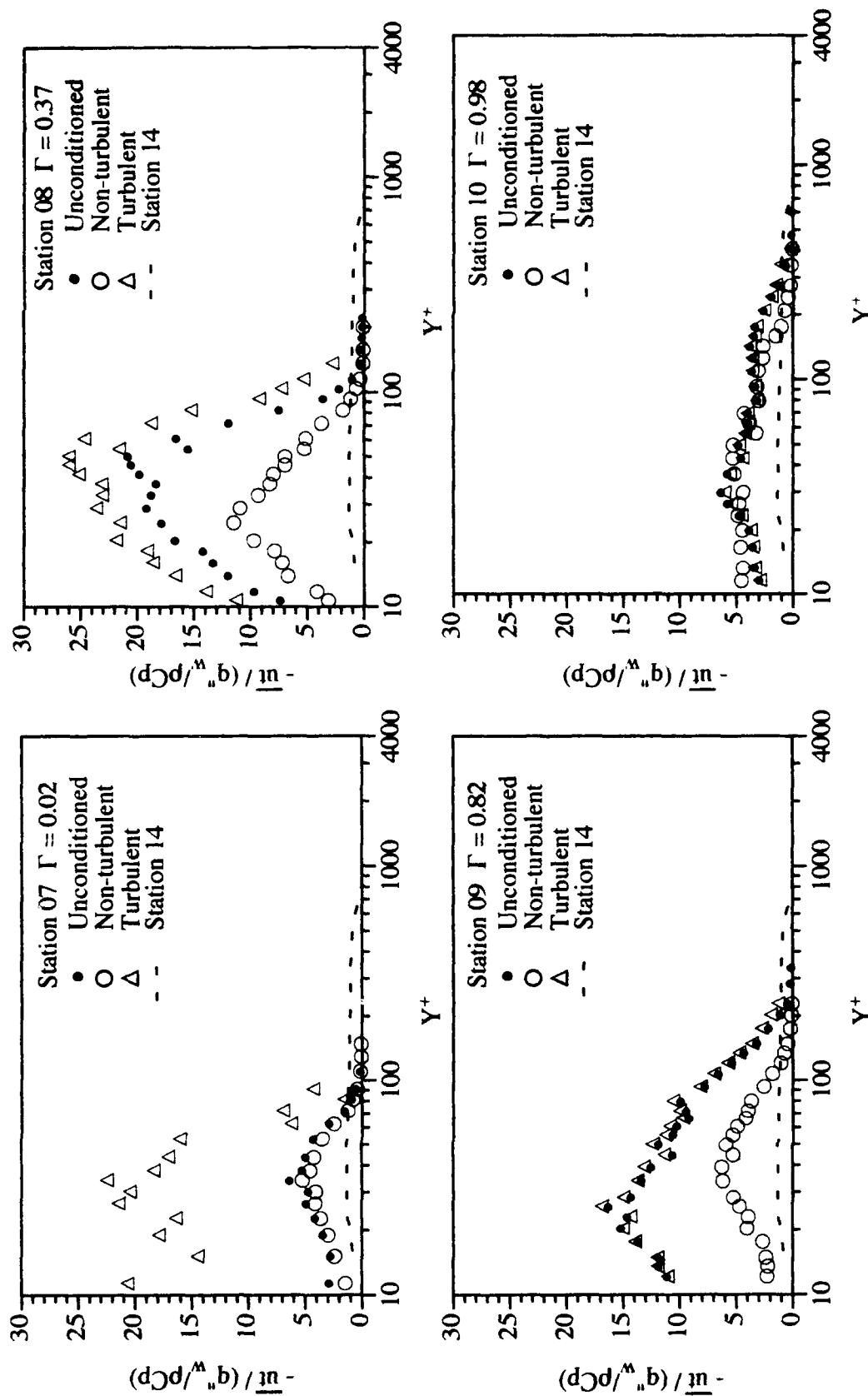


Figure 36 Conditionally sampled Reynolds streamwise heat flux for the K1 case (in wall units)
(Note: data points in the turbulent portion when $\Gamma < 0.005$ are omitted).

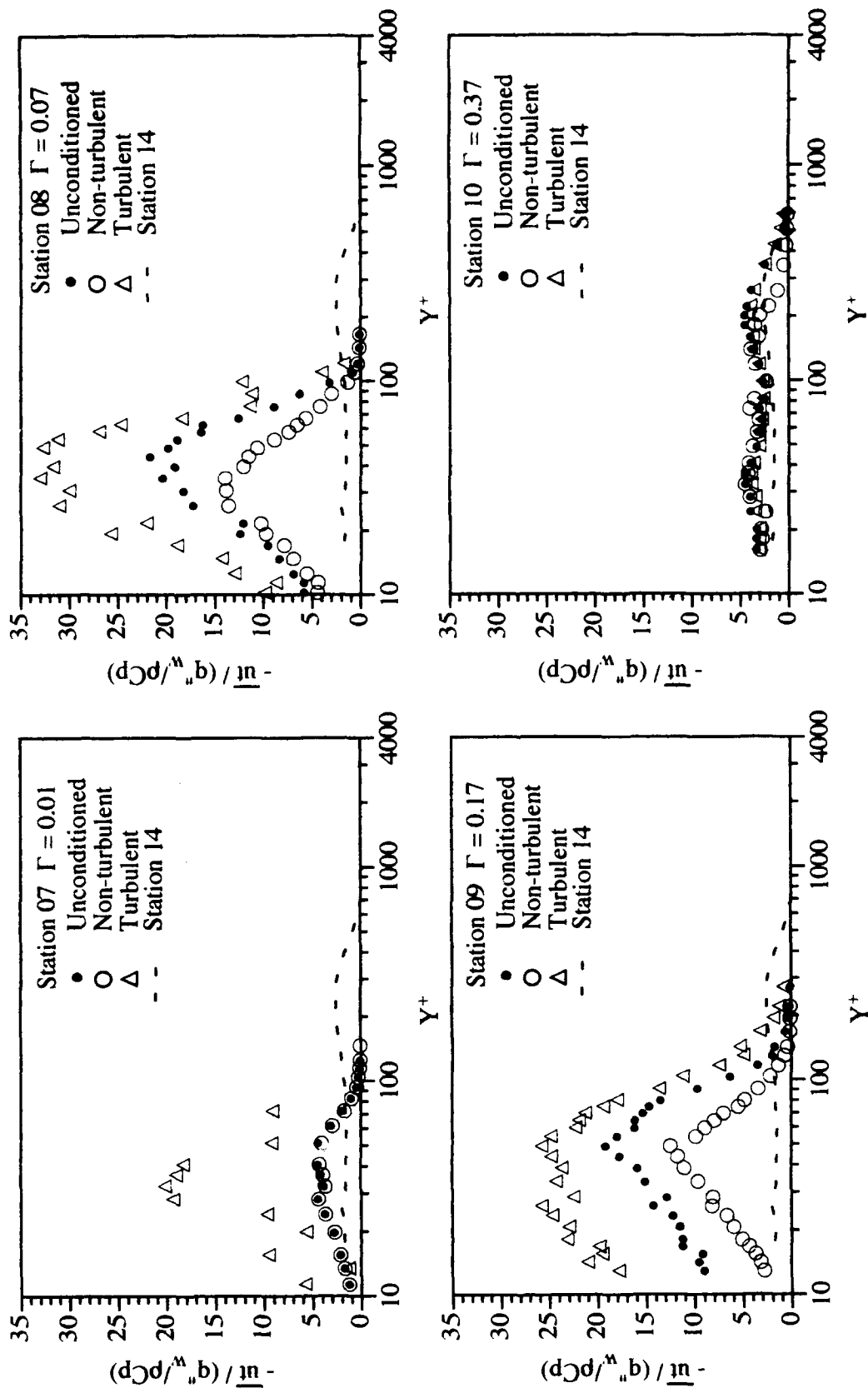


Figure 37 Conditionally sampled Reynolds streamwise heat flux for the K2 case, stations 07-10 (in wall units)
(Note: data points in the turbulent portion when $\Gamma < 0.005$ are omitted).

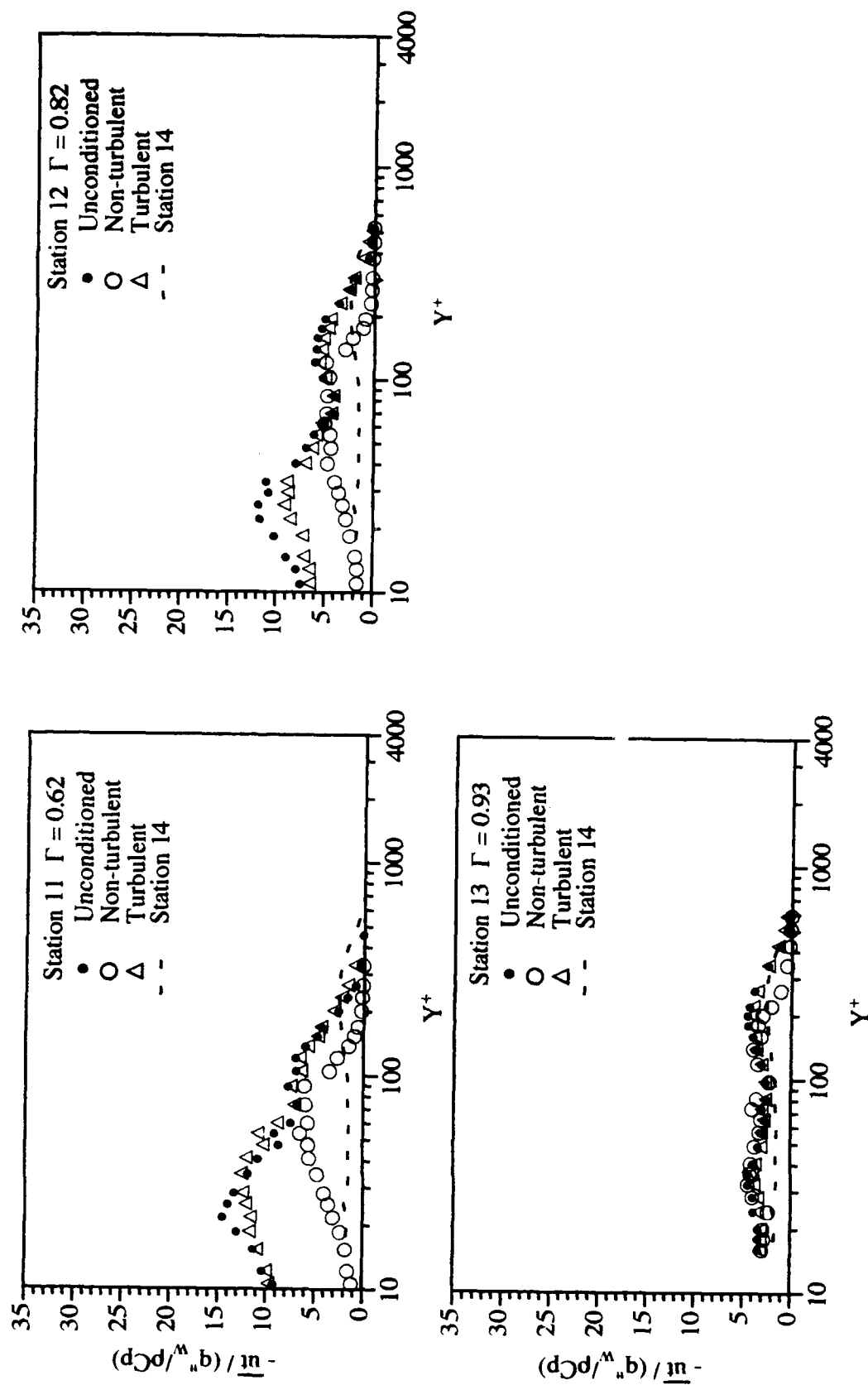


Figure 37 (Continued) (stations 11-13 in wall units) (Note: data points in the turbulent portion when $\Gamma < 0.005$ are omitted).